View metadata, citation and similar papers at core.ac.uk

brought to you by CORE

provided by NASA Technical Reports Server

NASA CONTRACTOR REPORT

NASA CR-1049

NASA CR-1
v.1
c.1

TECH LIBRARY KAFB, NM
0060428

LOAN COPY: RETURN TO
AFWL (WLIL-2)
KIRTLAND AFB, N MEX

BUCKLING OF SHELLS OF REVOLUTION WITH VARIOUS WALL CONSTRUCTIONS

Volume 1 - Numerical Results

by B. O. Almroth, D. Bushnell, and L. H. Sobel

Prepared by
LOCKHEED AIRCRAFT CORPORATION
Sunnyvale, Calif.
for Langley Research Center

NATIONAL AERONAUTICS AND SPACE ADMINISTRATION • WASHINGTON, D. C. • MAY 1968

TECH LIBRARY KAFB, NM
0060428

NASA CR-1049

BUCKLING OF SHELLS OF REVOLUTION WITH VARIOUS WALL CONSTRUCTIONS

Volume 1 — Numerical Results

By B. O. Almroth, D. Bushnell, and L. H. Sobel

Distribution of this report is provided in the interest of information exchange. Responsibility for the contents resides in the author or organization that prepared it.

Issued by Originator as Report 4-17-67-1

Prepared under Contract No. NAS 1-6073 by
LOCKHEED AIRCRAFT CORPORATION
Sunnyvale, Calif.

for Langley Research Center

NATIONAL AERONAUTICS AND SPACE ADMINISTRATION

For sale by the Clearinghouse for Federal Scientific and Technical Information
Springfield, Virginia 22151 – CFSTI price $3.00

FOREWORD

This is the first of three volumes of a final report entitled "Buckling of Shells of Revolution with Various Wall Constructions". The three volumes have the following titles:

Vol. 1 Numerical Results

Vol. 2 Basic Equations and Method of Solution

Vol. 3 User's Manual for BØSØR

The work described in these volumes was carried out under Contract NAS 1-6073 with the National Aeronautics and Space Administration.

ABSTRACT

Volume 1

Volume 1 presents the results of a parameter study performed with the computer program BØSØR (Buckling Of Shells Of Revolution) which is described in Volume 3. The axisymmetric collapse and the nonsymmetric bifurcation buckling behavior is studied for cylinders, cones, and spherical and toroidal shell segments subjected to axial compressive loads. Particular emphasis is placed on the effects of eccentricity in load application and on the influence of elastic end rings.

Volume 2

Volume 2 presents the equations on which the computer program BØSØR is based, as well as the method of solution of the equations. In addition, a set of more general stability equations is given in an appendix.

Volume 3

Volume 3 presents a comprehensive computer program (BØSØR) for the analysis of shells of revolution with axisymmetric loading. The program includes nonlinear prebuckling effects and is very general with respect to geometry of meridian, shell wall design, edge conditions, and loading. Despite its generality the program is easy to use. Branches are provided such that for commonly occurring cases the input data involves only basic information such as geometrical and material properties. The computer program has been verified by comparisons with other known solutions. The cards and a computer listing for this program are available from COSMIC, University of Georgia, Athens, Georgia, 30601.

NOTATION

A, B	refers to "A", "B" ends of shell meridian (see Fig. 1)
C_{11}	value of N_1 due to unit axial strain
e	load eccentricity (see Fig. 1)
EI_x	bending stiffness of edge ring about axis in the plane of the ring
GJ	torsional stiffness of edge ring
M_1	meridional bending moment
N_1	meridional stress resultant
n	circumferential waves in buckle pattern
P	total axial load
r	radius of edge ring
u	shell wall displacement
v	circumferential shell wall displacement
w	normal displacement component in buckling mode
β	meridional rotation

Subscripts

cr	critical value of the load
H	in horizontal (radial) direction
V	in vertical (axial) direction
o	prebuckling quantity
1	meridional direction
2	circumferential direction

Table of Contents

Section 1

INTRODUCTION

A few years ago researchers in the field of shell stability analysis had to be content with an analysis of highly idealized structures. In general only isotropic cylindrical or spherical shells were considered, and it was assumed that the membrane solution presented a sufficiently accurate approximation of the prebuckling state of stress. In addition the boundary conditions were usually simplified. The increasing efficiency of the digital computer has rapidly changed this situation. For a wide class of shells it is now possible to perform stability analyses without unduly restrictive approximations.

For axisymmetrically loaded shells of revolution the governing partial differential equations can be reduced to ordinary differential equations through separation of variables. An additional requirement for separation of variables is that the shell exhibits "orthotropic behavior". That is, in the prebuckling state axisymmetrical loads produce axisymmetrical displacements. By use of the numerical integration, finite difference, or finite element techniques, it is now practical to solve with reasonable accuracy almost any buckling problem for the type of shells discussed above. It is, for instance, easy to include in the buckling equations prebuckling quantities as they are obtained from a nonlinear analysis. While nonlinear equations were

used for instance by Weinitschke (Ref. 1) and Budiansky (Ref. 2) for the symmetrical snapping of spherical caps, the influence of the prebuckling displacements on bifurcation buckling was first recognized by Stein (Ref. 3) for cylindrical shells and by Huang (Ref. 4) for spherical caps. In cases such as that treated by Stuhlman, et al in Ref. 5 with edge moments introducing hoop stresses in the shell, it is imperative that an accurate prebuckling analysis be used. Other than cylindrical or spherical shells have been considered by Sobel and Flügge (Ref. 6), Bushnell (Refs. 7, 8) and by Cohen (Ref. 9) and others

Section 2
COMPUTER PROGRAM

In the present investigation, a computer program (BØSØR) has been derived for the elastic buckling of shells of revolution. A complete description of this computer program is given in Volume 3 ("User's Manual for BØSØR). The program can calculate axisymmetrical collapse loads as well as bifurcation buckling loads, the latter with either a membrane solution or an accurate nonlinear solution for the prebuckling displacements. The program is easy to use but still general with respect to

1. geometry of meridian
2. type of wall construction
3. type of boundary conditions
4. type of loading

These objectives have been achieved through provision of program branches with minimum input in addition to the branch for the most general case.

For the geometry of the meridian the general branch of the computer program calls for input in the form of cartesian coordinates for a number of points along the meridian. Special branches are provided for cylindrical, conical, spherical, and toroidal shells.

The general branch for the shell wall stiffness data calls for input in the form of coefficients of the constitutive equations. Special branches

calling for simpler input data are provided for

1. shells with ring and stringer stiffening
2. shells with skew stiffeners
3. fiber reinforced (layered) shells
4. layered shells (isotropic or orthotropic)
5. corrugated ring stiffened shells
6. shells with one corrugated and one smooth skin (with rings)

The stiffness coefficients must be constant along the meridian.

The most general form of the boundary conditions for the prebuckling analysis is a set of four nonhomogeneous equations containing twenty coefficients. For the stability analysis, the homogeneous boundary conditions consist of eight equations with sixty-four coefficients. The general branch of the computer program calls for all these coefficients as input. Several branches are provided, however, through which the boundary conditions are calculated internally with only control integers required as input. These branches include force or displacement boundary conditions, support by elastic edge rings, or support by an elastic medium. The shell can be open or closed at the apex.

The following types of axially symmetric loading conditions are considered

1. uniform normal pressure
2. axial line loads at ends of shell
3. combination of uniform normal pressure and axial line loads (which vary proportionally as the load is increased)

The axial load need not be applied at the neutral surface of the shell .

The coefficients of the constitutive equations and more details on the boundary conditions are given in Volume 2 of this report.

As formulated in the computer program the analysis has two parts: In the first part the two equations governing the prebuckling state of the shell are solved. These are nonlinear, nonhomogeneous, second-order ordinary differential equations. They were originally derived by Reissner (Ref. 10). The Newton-Raphson procedure is used to solve the set of nonlinear algebraic equations which result from a finite-difference analog of the differential equations. The solution of the equations governing the prebuckled equilibrium state yields the prebuckling meridional rotation and meridional and circumferential stress resultants. These quantities appear as known variable coefficients in the equations governing the stability of the equilibrium state.

In the second part of the analysis the stability equations (Donnell type formulation) are solved. There are two linear, homogeneous, fourth-order, partial differential equations for each mesh point. Dependence on the circumferential coordinate can be eliminated as the dependent variables are harmonic. The resulting ordinary differential equations are solved by the method of finite-differences. The stability analysis is formulted as an eigenvalue problem with the lowest eigenvalue of the stability equations corresponding to the critical load. The prebuckling and stability equations are given in Volume 2.

The computer program has been used for the stability analysis of eccentrically stiffened cylinders, conical frustrums, and spherical and

toroidal segments. Comparisons have been made with the test results of Refs. 5 and 11 through 16.

Section 3
NUMERICAL RESULTS

The computer program discussed above has been verified through comparison to previously known analytical or numerical solutions. It has been applied also to a number of cases for which experimental analyses are available. Some important points are revealed through comparison of theoretical and experimental results. In addition certain special effects have been studied for stiffened cylindrical, conical, spherical and toroidal shells. The parameter study has been concerned with the type of shell specimens which is considered in Ref. 5. The geometry for the different shells investigated is shown in Fig. 1.

The accuracy in the numerical results depends on the number of points in the finite difference mesh. Due to computer storage limitations this number is not allowed to exceed 100. This appears to be sufficient for most practical applications. Another complication is that with a large number of points numerical difficulties may arise. Introduction of double precision programming to overcome these difficulties would have to be compensated by a restriction in the number of mesh points and thus would severely limit the scope of the program. In a typical case, as the number of points is increased, the corresponding critical load appears to approach a certain limit; further

increase may result in somewhat erratic values of the critical load. Typical examples are shown in Tables 1a and 1b. The results of Table 1b are plotted in Fig. 2. For short shells numerical difficulties generally occur at a lower value of the number of points. However, in these cases fewer points are needed. For cases in which the length of the shells shown in Fig. 1 is increased by a factor of four, no numerical difficulties occur at or below the maximum number of points. Due to this fortunate state of affairs it has been possible to obtain quite accurate results in almost all cases for which a solution has been attempted. Exceptions to this are shells with free edges or weak end rings, for which the buckling pattern is almost inextensional.

3.1 Comparison to Other Theoretical Analyses

For monocoque cylinders under hydrostatic pressure, the buckling loads obtained are in complete agreement with those given by Sobel (Ref. 17). For monocoque cylinders under axial compression a comparison was made with the results of Ref. 18. For shells with $L/R = 0.7$ and $R/t = 100$ and the boundary conditions S1, S4, and C2 (in the notations of Ref. 18), the normalized critical loads are 0.869, 0.506, and 0.858. The corresponding results presented in Ref. 18 are 0.876, 0.508, and 0.863. The difference (less than one percent) is probably due to the use of a larger number of mesh points and double precision arithmetic in Ref. 18. In Ref. 5 buckling loads are given for the type of cylindrical shells shown in Fig. 1. Corresponding results for cylinders 95 inches long were computed with the present program

and the agreement is reasonably good. The results of Ref. 5 are somewhat higher (up to 10%) which could well be due to the fact that it is based on a one term Galerkin solution. Critical loads were computed also for spherical shell segments under tension. The results were compared to the theoretical results presented by Yao in Ref. 19. The present results were 2% to 3% lower than those obtained by Yao. For comparison with results presented in Ref. 20 the critical load was also computed for two simply-supported[a] toroidal segments. For a segment with positive Gaussian curvature and external stiffeners, the critical tension load according to Ref. 20 (in which linear membrane prebuckling theory is used) is 17788 lbs/in. at the equator. If a membrane prebuckling analysis is used for the same segment the present program gives 17745 lbs/in and with the more accurate nonlinear prebuckling analysis a critical tension load of 18383 lbs/in is obtained. The agreement between the two analyses is good, and the influence of nonlinearity in the prebuckling analysis is rather small. For a toroidal segment with negative Gaussian curvature, Ref. 20 gives a critical compression load of 1913 lbs/in. The present analysis gives 1690 lbs/in with membrane prebuckling analysis and 1686 lbs/in with nonlinear prebuckling theory.

3.2 Comparison to Test Results

Results from the present analysis compare well to test results for cylinders of 95 inch length loaded through the center of the skin (Ref. 5). Three

---

[a] "Simple-support" implies $N_1 = M_1 = u_H = v = 0$
"Clamped" implies $u_H = \beta = v = u_V = 0$

separate tests gave buckling loads of 3440, 3550, and 3650 lbs/in, while the computer program indicates a critical load of 3505 lbs/in.

A large number of stiffened cylinders were tested by Milligan et al, Ref. 11. They also calculated the critical load and concluded that for stiffened cylinders, theory and experiment are in agreement. The ratio between experimental and theoretical loads varies according to Ref. 11 from .81 to 1.28. One of the reasons for the surprisingly high values of this ratio is that the theoretical analysis underestimates the stiffness of the shell wall. The assumption is made that the stiffeners do not contribute to the bending or extensional stiffness perpendicular to the stiffener direction. Also in some cases the assumption of simple support results in theoretical values which are too low. The present computer program was used to calculate the critical loads for some of the cylinders for which test results are reported in Ref. 11. The theoretical and the experimental loads of Ref. 11, as well as the loads from the present program, are given in Table 2. With membrane prebuckling analysis, results are given both for simply-supported and for clamped cylinders. Results with nonlinear prebuckling analysis are given only for clamped shells. The shells tested by Milligan, et al (Ref. 11) had rather insignificant stiffening. Therefore, it appears that their behavior should not be too different from that of monocoque shells. It is noticed that the relation between results from the present theory and from the tests of Ref. 11 is in accordance with the experience for monocoque shells.

In Table 3 theoretical loads for some fiber wound cylinders are compared to experimental loads reported in Refs. 12, 13, and 14. Results obtained with

membrane analysis are shown both for cylinders with simply supported and with clamped ends. With the nonlinear prebuckling analysis critical loads were obtained for clamped shells. It can be seen that the influence of nonlinearity in the prebuckling analysis and the influence of rotational edge restraint tend to cancel one another. The experimental results for fairly thick cylinders were not included in the comparison. It appears that buckling of thick cylinders is precipitated by a shear failure in the matrix. With one exception experimental results range between 62 and 85 percent of the theoretical results.

Card and Jones (Ref. 15) tested stringer stiffened cylinders with wall thickness such that agreement between test and theory is to be expected. For cylinder No. 3 in Ref. 15, the present program gives for simple support edge conditions critical loads of 1378 lbs/in with membrane prebuckling analysis and 1451 lbs/in with nonlinear prebuckling analysis. If the cylinder is considered clamped the corresponding buckling loads are 2657 lbs/in and 2644 lbs/in. For the test specimen the edge conditions were probably reasonably close to complete clamping. The cylinder buckled at 2120 lbs/in.

For ring stiffened conical shells under axial compression some test results are given in Ref. 16, together with an approximate formula for the critical load. For the specimens designated 3-3 and 3-3A in Ref. 16, the critical axial load according to the formula is 7510 kg. According to the present theory axially symmetric buckling is critical. Buckling loads for the two specimens are 6480 kg and 7100 kg respectively. The experimental results are 5800 kg and 6000 kg.

3.3 Effect of Load Eccentricity

The effect of eccentricity in the load application was studied for shells such as those shown in Fig. 1. Results for cylindrical and conical shells are shown in Table 4. Critical axial loads were computed for the cases in which the shells are simply supported at the midsurface of the skin, at the neutral surface of the cross-section and at the midpoint of the rectangular stiffeners. Clamped shells were also considered. For each type of loading critical loads were obtained both for shells with external and with internal stiffening. The analysis is based on a finite difference mesh size equal to 1/50 of the shell length.

For comparison, critical loads are shown also as computed by use of the membrane analysis. With a membrane prebuckling analysis and in the absence of axial restraint there is no loading eccentricity effect. The results from the first three loading cases are identical.

It may be seen from Table 4 that the effect of the cone angle is small. On the other hand, changes in the loading eccentricity have drastic effects on the critical load. For the case in which the shell is loaded through its neutral surface, for example, it is interesting to compare results obtained with membrane prebuckling analysis to those obtained with nonlinear prebuckling analysis. The difference here is due to the Poisson expansion in connection with radial restraint at the edges. This effect is surprisingly large, particularly for shells with outside stiffening.

For shells with end moments it is easy to see that the presence of a moment which tends to bend the cylinder into a barrel shape greatly increases the critical load. A moment in the other direction, developing prebuckling compressive hoop stresses, has the opposite effect. Prebuckling displacements (u_{Ho}) and buckling modes (w) are shown for cylinders with inside stiffening in Figs. 3 and 4. Fig. 3 corresponds to loading through the neutral surface and Fig. 4 to loading through the center of the stiffeners. Fig. 5 shows prebuckling displacements and buckling modes for conical shells which are either clamped or simply supported and loaded through the center of the skin.

For the cylindrical and conical shells, bifurcation occurs at loads which are small fractions of the loads at which axisymmetrical collapse would occur. For axially compressed spherical and toroidal segments, such as shown in Fig. 1, bifurcation buckling usually occurs close to the collapse loads. The prebuckling displacements are then very large.

Table 5 gives buckling loads for axially compressed, eccentrically stiffened spherical and toroidal segments (See Fig. 1). Two loads are given for each case, a load corresponding to bifurcation buckling ($n \neq 0$) and a load corresponding to axisymmetric collapse ($n = 0$). The spherical and toroidal segments with external stiffeners buckle nonsymmetrically at lower loads than those with internal stiffeners. Eccentrically stiffened cylindrical and conical shells exhibit the opposite behavior. This is not so surprising since nonsymmetric buckling occurs at loads which are close to the axisymmetric collapse load. The collapse load is found to be higher for shells with inside stiffeners. The critical wave number for toroidal segments is higher

than that for spherical segments. In the case of a toroidal segment with the load applied through the center of the outside stiffeners, the resulting meridional end moments cause considerable hoop compression near the edges. The critical wave number (65) in this case, is far above the others because buckling is primarily due to this hoop compression. Similar hoop stresses occur for spherical shells and also for shells with inside stiffening loaded through the center of the skin. In these cases, however, the buckling load corresponding to critical axial compression is still lower.

Figure 6 gives a prebuckling load-deflection curve for a spherical segment with internal stiffeners. The load is applied at the middle surface of the skin (shear center). This figure illustrates the method in which a collapse load is calculated. The axisymmetric prebuckling displacements and stresses are first calculated for $P/2\pi C_{11} = 0.3$. The load is increased in increments of $P/2\pi C_{11} = 0.1$ until at $P/2\pi C_{11} = 0.7$ the Newton-Raphson process fails to converge. The step size is then decreased and $P/2\pi C_{11}$ set equal to 0.6 plus the new increment. At $P/2\pi C_{11} = 0.82$ the prebuckling solution again fails to converge, and the step size is again decreased. Calculations continue in this manner until the step size is smaller than some pre-assigned value (in this case .001 of the initial step size) at which point they terminate. The shell is judged to have collapsed axisymmetrically at the highest value of the load for which a solution was obtained.

With too large an initial step size it is possible to jump over a collapse load and find solutions to the prebuckling equations on another branch which may or may not represent unstable equilibrium. Such an upper branch

is shown in Fig. 6. The sign of the stability determinant for n = 0 generally changes from one branch to another, but the stability determinant for $n \neq 0$ does not necessarily change sign. When calculating buckling loads for $n \neq 0$, one must make the initial step size small enough to guarantee that a collapse load is not bypassed in the search for the lowest bifurcation load.

Figure 7 shows a prebuckling load-deflection curve for a spherical segment with external stiffeners, with the load applied through the centroid of the stiffeners. Two branches are shown, and the deflection patterns $u_{Ho}(s)$ associated with each branch are indicated.

Figure 8 gives displacements corresponding to the two branches of the load-deflection curve plotted in Fig. 6. Collapse occurs at $P/2\pi C_{11} = 0.814$. The upper branch (dotted lines) represents unstable equilibrium, since an increase in load corresponds to a decrease in displacement.

Figure 9 shows the buckling mode for the shell, for which the prebuckling behavior is shown in Figs. 6 and 8. The shell buckles into 8 waves at a load about 20% below the collapse load (See Table 5).

Figures 10 and 11 show the prebuckling displacements and buckling mode shape for a clamped spherical segment with internal stiffeners. It is noted that again there are two branches of the prebuckling load-deflection curve. The shell collapses at $P/2\pi C_{11} = 1.05$, but solutions of the prebuckling equilibrium equations exist for higher loads than this. In Fig. 10 it can be seen that the upper branch represents stable equilibrium, that is deflection increases with load.

Figures 12 and 13 show the prebuckling behavior and buckling mode of a clamped spherical segment with external stiffeners. Again, the prebuckling displacements correspond to two branches of the load-deflection curve. In this case the upper branch is unstable. The shell buckles into 6 circumferential waves at a load not far below the collapse load.

Figures 14 through 18 present numerical results for eccentrically stiffened toroidal segments (See Fig. 5 for geometry). In Fig. 14 are shown load-deflection curves for internally stiffened toroidal segments loaded at the shear center, the neutral surface, and the centroids of the stiffeners. For all three cases the collapse loads are fairly close.

Figures 15 and 16 show the prebuckling radial displacements for externally stiffened toroidal segments loaded respectively through the neutral surface and through the centroid of the stiffeners. Shells loaded through the neutral surface tend to deflect outward near the edge and inward near the equator. The large meridional bending moment caused by loading the shell through the centroid of the external stiffeners forces it to deflect inward near the edge and outward near the equator.

Figures 17 and 18 present prebuckling and buckling displacements for the same cases for which prebuckling data are presented in Figs. 15 and 16. There are two buckling modes shown in Fig. 17, one corresponding to n = 10 and one corresponding to n = 70. This particular case exhibits two minima in the curve P_{cr} versus n. The minimum at n = 10 corresponds to buckling in which the primary cause is the compressive meridional stress resultant N_{10}. The somewhat higher minimum at n = 70 corresponds to buckling in which the primary

cause is the compressive prebuckling hoop stress resultant N_{20} at the equator.

Figure 18 shows the prebuckling and buckling displacements for the externally stiffened toroidal segment loaded through the centroids of the stiffeners. The large meridional bending moment thus produced causes hoop compression to develop near the edge, and this compression causes buckling into a high number of circumferential waves. As in the previous case, this case exhibits two minima in the curve P_{cr} versus n. However, the minimum at the higher wave number 65 is the lower of the two. The corresponding buckle pattern is very different from that for n = 70 shown in Fig. 17, because the maximum hoop compression occurs near the edge rather than at the equator.

3.4 Shells with Edge Rings

Bifurcation buckling of eccentrically stiffened shells with edge rings falls into two classes: If the edge rings are not very stiff, the shells buckle almost inextensionally with n = 2 at loads which can be many orders of magnitude smaller than the buckling loads for clamped shells. Cohen (Ref. 21) found such loads for axially compressed monocoque cylindrical shells. If the ring stiffness exceeds some critical value (see Fig. 19), the shells buckle with n > 2 at loads comparable to the buckling loads for clamped edges, and the buckle pattern is no longer inextensional.

Figure 19 shows the critical axial loads for an internally stiffened 5° cone supported by edge rings of square cross-section. The centroid of the rings coincides with the shear center of the shell wall. The length of the

cone is 95 inches and the radius of the parallel circle at the mid-length is 198 inches. From Fig. 19 it is seen that shells with edge rings less than 9.4 inches thick buckle with n = 2 at loads which decrease sharply as the size of the ring decreases. For rings larger than 9.4 inches in thickness , the shell buckles with n = 20 at loads very near that for clamped edges. The buckling load corresponding to simply-supported edges is also shown in the figure.

Figure 20 shows the modal displacements of the "inextensional" (n = 2) mode for ring thicknesses t_r of 2.608 and 7.824 inches. Modal displacement u_H and v are shown. For t_r = 2.608 the generators remain practically undeformed during buckling. The thicker ring t_r = 7.824 clearly forces the generators to deform during buckling.

Figure 21 shows normalized buckling loads for ring-supported conical shells versus the number of meridional stations in the finite-difference scheme. The loads are normalized by P_{limit} , the value that P seems to approach as the number of meridional stations is varied. For small rings it is clear that numerical difficulties occur with increasing numbers of points before convergence has been achieved. It appears that the problem as formulated in the stability equations is ill conditioned for the case in which the generators remain undeformed (inextensional buckling).For rings with t_r = 2.608 , 3.912 , and 5.216 the solution has stabilized before numerical difficulties occur.

Figure 22 shows buckling loads for ring-supported spherical segments of the geometry shown in Fig. 1 The "inextensional" mode (n = 2) is antisymmetric about the midlength of the segment; the mode corresponding to bifurcation of clamped segments is symmetric about the midlength. The curve for antisymmetric buckling (n = 2) crosses that for symmetric buckling (n = 6) at values of t_r which are surprisingly large.

Figure 23 is similar to Fig. 21: It shows the convergence properties of the "inextensional" (n = 2) buckling mode with number of meridional stations on the spherical segment. Again, convergence improves as the ring size increases.

For a cylindrical shell the influence of an end ring is studied for the case in which the inextensional pattern is suppressed through use of edge support. The ring is fixed at its centroid in the axial, circumferential, and radial directions, but is free to rotate. The results are shown in Fig. 24. The somewhat peculiar form of the curve emphasizes a phenomenon which is often overlooked: there are two sets of boundary conditions which effect the buckling load, that governing the axisymmetric prebuckling behavior, and that governing nonsymmetric buckling. In the present example the ring cross-section is allowed to rotate only. If the stiffness K is defined as the edge moment per unit rotation applied by the ring to the shell, then for axisymmetric prebuckling deformation $K_p = EI_x/r^2$, and for harmonic buckling deformations with n waves $K_b = (EI_x + n^2GJ)/r^2$. In this case the bending stiffness EI_x is approximately equal to the torsional stiffness GJ, and the wave number n is large. Hence K_b is much bigger than K_p, which gives rise to two regions

in the curve of Fig. 24. When t_r is less than about 3 inches the increase in critical load with ring size is due primarily to the increase in the ring torsional stiffness, which governs the restraint against edge rotation in the buckling mode. This observation is supported by the curve in Fig. 24 labeled "Membrane Prebuckling Analysis". The curve rapidly approaches an asymptote which corresponds to clamped shells. When t_r is greater than about 3 inches, the increase in critical load with ring size is due primarily to the increase in the ring bending stiffness, which governs the restraint against edge rotation in the prebuckling phase. In comparison to the results presented in Ref. 21 and 22 a very heavy ring is needed before clamped conditions are approached. This is of course connected with the fact that the shell considered here is very short and has a large bending stiffness in the axial direction. The value of the critical load for zero ring thickness is not the same as the value for simple support, since "simple support" implies no axial restraint. The presence of axial restraint increases the critical load from 3020 to 4588 lbs/in.

REFERENCES

1. Weinitschke, H., "On the stability problem for shallow spherical shells", J. Math. and Phys. 38, 209-231, (1960)

2. Budiansky, B., "Buckling of clamped shallow spherical shells," Proc. I.U.T.A.M. Symp. of Theory of Thin Elastic Shells, Amsterdam, North-Holland Publishing Co., 1960, pp. 64-94

3. Stein, M.,"The effect on the buckling of perfect cylinders of prebuckling deformations and stresses induced by edge support," Collected Papers on Instability of Shell Structures, NASA TN D-1510, p. 217 (1962)

4. Huang, N-C, "Unsymmetrical buckling of thin shallow spherical shells," J. App. Mech., 31, 447-457, (1964)

5. Stuhlman, C., DeLuzio, A., and Almroth, B., "Influence of stiffener eccentricity and end moment on stability of cylinders in compression," AIAA J., 4, 872-877, (1966)

6. Sobel, L. H. and Flügge, W., "Stability of toroidal shells under uniform external pressure," AIAA J., 5, 425-431, (1967)

7. Bushnell, D., "Nonlinear analysis of shells of revolution", Lockheed Missiles and Space Co. Rept. 6-67-66-6, April 1966, also AIAA J., 5, 432-439 (1967)

8. Bushnell, D., "Symmetric and nonsymmetric buckling of finitely deformed eccentrically stiffened shells of revolution", Lockheed Missiles and Space Co., Rept. 6-67-66-15, August 1966, also AIAA J., 5, (1967)

9. Cohen, G. A., "Computer analysis of asymmetric buckling of ring-stiffened orthotropic shells of revolution," presented at the AIAA 5th Aerospace Sciences Meeting, New York, Jan. 1967, AIAA Paper No. 67-109

10. Reissner, E., "On axisymmetrical deformation of thin shells of revolution," Proc. of Symposia in Applied Mathematics, Vol. III, (McGraw-Hill, 1950) p. 45-46

11. Milligan, R., Gerard, G., Lakshmikantham, C., and Becker, H., "General instability of orthotropically stiffened cylinders," Techn. Rept. AFFDL TR 65 161, Wright-Patterson Air Force Base, July 1965

12. Ravenall, R., "Designing for stiffness and buckling in filament-wound rocket case structures," AIAA Launch and Space Vehicle Shell Structures Conference, April 1963

13. Tasi, J., Feldman, A., and Stang, D. A., "The buckling strength of filament-wound cylinders under axial compression," NASA CR-266, July 1965

14. Card, M. F. and Peterson, J. P., "On the instability of orthotropic cylinders," NASA TN D-1510, pp. 297-308, 1962

15. Card, M. F. and Jones, R. M., "Experimental and theoretical results for buckling of eccentrically stiffened cylinders," NASA TN D-3639, Oct. 1966

16. Singer, J., Berkovits, A., T. Weller, O. Ishai, M. Baruch, and O. Harari, "Experimental and theoretical studies on buckling of conical and cylindrical shells under combined loading," TAE report No. 48, Technion Research and Development Foundation, Haifa, Israel, 1966

17. Sobel, L. H., "Effect of boundary conditions on the stability of cylinders subject to lateral and axial pressures," AIAA J., 2, 1437-1440, (1964)

18. Almroth, B. O., "Influence of edge conditions on the stability of axially compressed cylindrical shells," AIAA J., Vol. 4, No. 1, Jan 1966

19. Yao, J. C., "Buckling of a truncated hemisphere under axial tension," AIAA J. 1, 2316-2319 (1963)

20. McElman, J. A., "Eccentrically stiffened shallow shells of double curvature," NASA TN D-3826, Feb 1967

21. Cohen, G. A., "Buckling of axially compressed cylindrical shells with ring-stiffened edges," AIAA J., 4, 1859-1862, (1966)

22. Almroth, B. O., "Influence of imperfections and edge restraint on the buckling of axially compressed cylinders," NASA CR-432, April 1966

Table 1a Critical Axial Load as Function of Mesh Size (Shells shown in Fig. 1)

10° Cone Loaded through Skin Simply Supported[a] External Stiffening	
NUMBER OF MERIDIONAL INTERVALS	CRITICAL LOAD 10^{-3} P_{cr}
19	4006
29	4010
39	4013
49	4013
59	4015
69	4014
79	4041
89	4220
99	4185

[a]"Simple Support" implies $M_1 = N_1 = u_H = v = 0$

Table 1b Critical Axial Load as Function of Mesh Size (Shells shown in Fig. 1)

Cylinder Clamped[a] External Stiffening	
NUMBER OF MERIDIONAL INTERVALS (ON HALF LENGTH)	CRITICAL LOAD N_{cr}
15	7742
17	7757
20	7771
21	7774
23	7780
25	7782
27	7788
28	7788
29	7791
30	7797
31	7788
33	7794
35	7795
37	7801
40	7777
45	7823

[a]"Clamped" implies $u_H = \beta = v = u_V = 0$

Table 2 Buckling Loads of Stiffened Cylinders

Cyl. No.	Theory Ref. 11	Membrane Prebuckling		Nonlinear Prebuckling	
		Simple Support	Clamped	Clamped	Experiment Ref. 11
13	228	283	337(15)[a]	293(14)	185
14	239	265	345(14)	302(14)	206
15	265	321	335(14)	303(14)	230
16	318	382	386(13)	346(13)	268
22	92	117	158(16)	157(16)	99
23	101	124	173(15)	169(14)	96
24	207	246	298(15)	290(14)	204
25	178	221	226(15)	203(16)	160
26	252	289	317(13)	311(12)	244
27	285	337	410(14)	406(12)	234
28	131	153	206(15)	186(15)	117
31	282	345	351(15)	325(14)	228
36	316	364	383(14)	366(13)	256
38	265	333	338(15)	330(14)	231
41	290	354	418(13)	408(12)	297
43	117	146	200(14)	202(14)	150

[a] Buckling loads in lbs/in
Numbers in parens indicate critical wave numbers.

Table 3 Buckling of Fiber Reinforced Cylinders

Ref.	No.	Membrane Prebuckling		Nonlinear Prebuck. Clamped	Experiment
		Simple Support	Clamped		
12	1	710	711	699(11)[a]	598
"	2	1035	1045	1028(10)	765
"	3	1203	1211	1181(10)	850
"	4	1289	1293	1241(10)	775
13	3	469	469	463(11)	337
"	4	473	473	466(11)	373
"	6a	330	330	325(13)	272
"	7a	318	318	314(13)	335
"	9	248	248	245(15)	200
14	1	726	728	713(11)	609
"	2	726	728	713(11)	622
"	3	726	728	713(11)	629
"	4	726	728	713(11)	650

[a] Buckling loads in lbs/in
Numbers in parens indicate number of circumferential waves in buckle pattern

Table 4 Buckling Loads (millions of lbs.) for Eccentrically Stiffened Aluminum Cylindrical and Conical Shells

BOUNDARY CONDITION CODE NO[a]		INTERNAL STIFFENING			EXTERNAL STIFFENING		
		CYL	5° Cone	10° Cone	CYL	5° Cone	10° Cone
Nonlinear Pre-buckling Analysis	1	1.670 (18)[b]	1.650 (18)	1.600 (18)	3.770 (19)	3.730 (19)	3.620 (18)
	2	1.250 (20)	1.240 (19)	1.200 (19)	4.350 (17)	4.300 (17)	4.160 (17)
	3	3.580 (14)	3.540 (14)	3.480 (14)	1.235 (26)	1.235 (16)	1.200 (26)
	4	4.540 (20)	4.480 (20)	4.330 (19)	9.620 (15)	9.570 (15)	9.100 (15)
Membrane Pre-buckling Analysis	1,2,3	1.520 (18)	1.485 (18)	1.440 (18)	2.700 (21)	2.640 (21)	2.570 (20)
	4	3.670 (21)	3.820 (21)	3.620 (21)	6.060 (22)	5.920 (22)	5.740 (22)

[a]Boundary Condition Code: Axial load applied at
1. neutral surface
2. shear center
3. centroid of stiffener
4. shell clamped

[b]Numbers in parens indicate number of circumferential waves in buckle pattern

Table 5 Buckling Loads (lb/in at equator) for Eccentrically Stiffened Aluminum Spherical and Toroidal Segments

BOUNDARY CONDITION CODE NO.[a]		INTERNAL STIFFENING		EXTERNAL STIFFENING	
		SPHERE	TORUS	SPHERE	TORUS
Bi-furcation	1	9190 (8)[b]	9090 (11)	7200 (8)	7300 (10)
	2	9650 (8)	10000 (10)	6900 (8)	6800 (11)
	3	8280 (9)	7620 (11)	no bifurcation	5650 (65)
	4	12880 (6)	12900 (7)	10500 (6)	10670 (7)
Collapse	1	10100 (0)	10720 (0)	7690 (0)	8250 (0)
	2	10250 (0)	10950 (0)	7575 (0)	8150 (0)
	3	9650 (0)	10400 (0)	8400 (0)	8540 (0)
	4	13250 (0)	13400 (0)	11400 (0)	11040 (0)

[a]Boundary Condition Code: Axial load applied at
1. neutral surface
2. shear center
3. centroid of stiffener
4. shell clamped

[b]Numbers in parens indicate number of circumferential waves in buckle pattern.

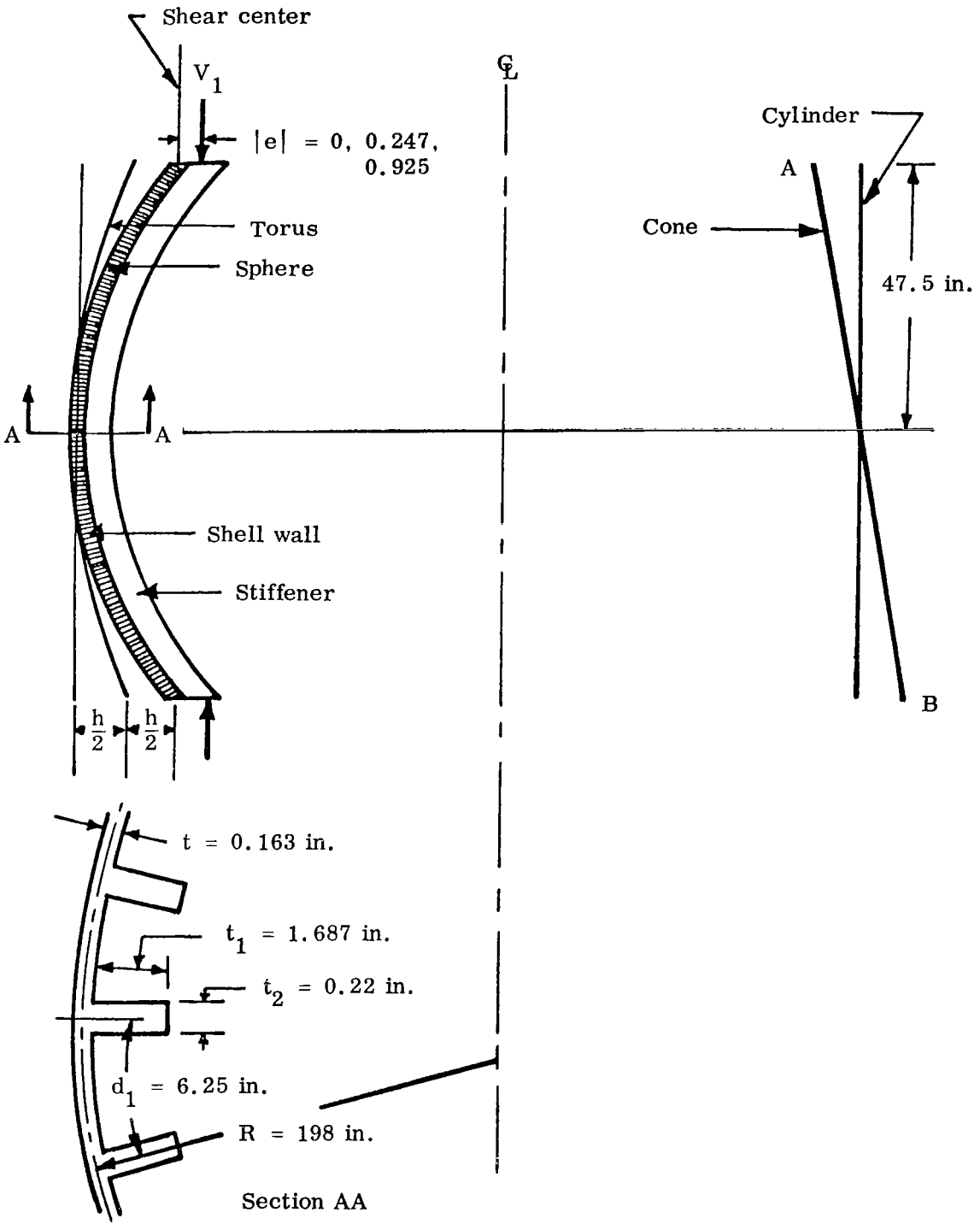

Fig. 1 Geometry of cylinders, cones, spherical segments, and toroidal segments

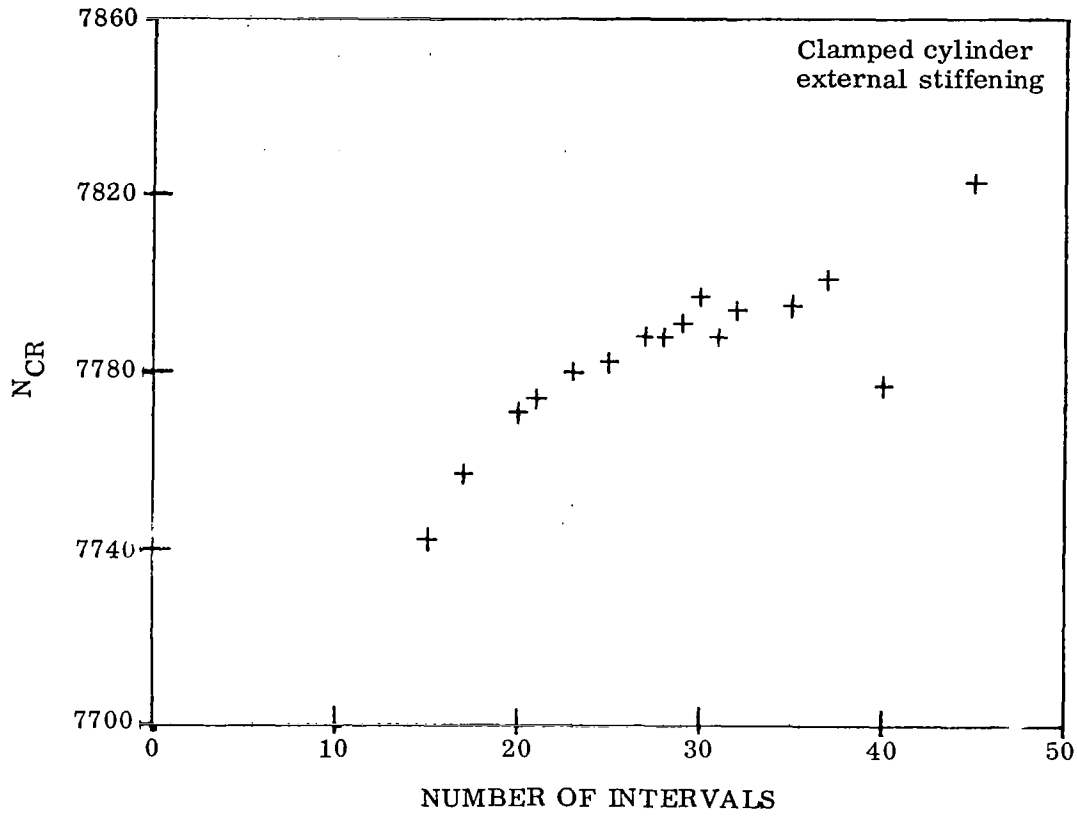

Fig. 2 Critical Axial Load as function of mesh size for cylinder shown in Fig. 1

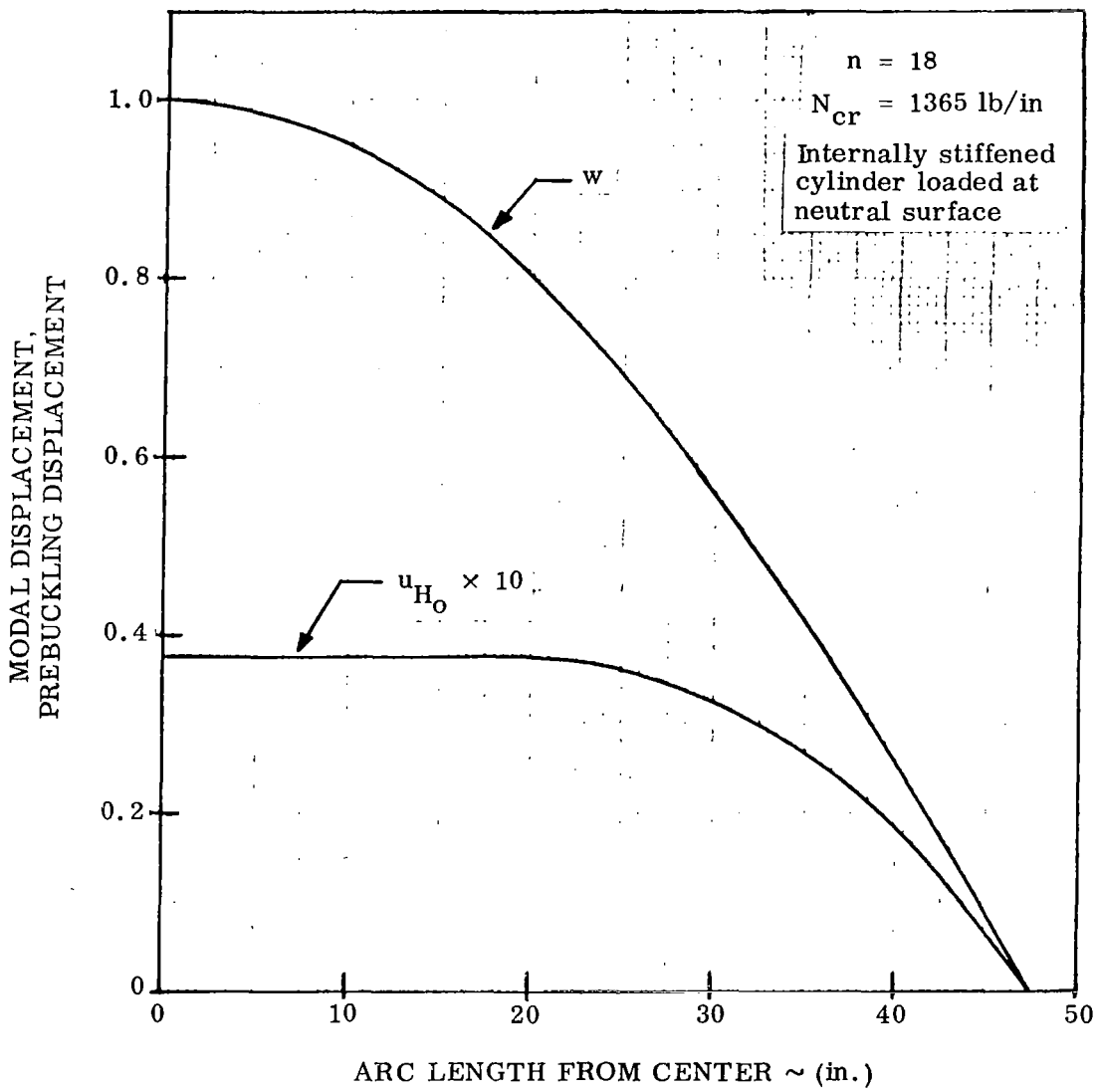

Fig. 3 Prebuckling and buckling displacements of an internally stiffened simply supported cylinder

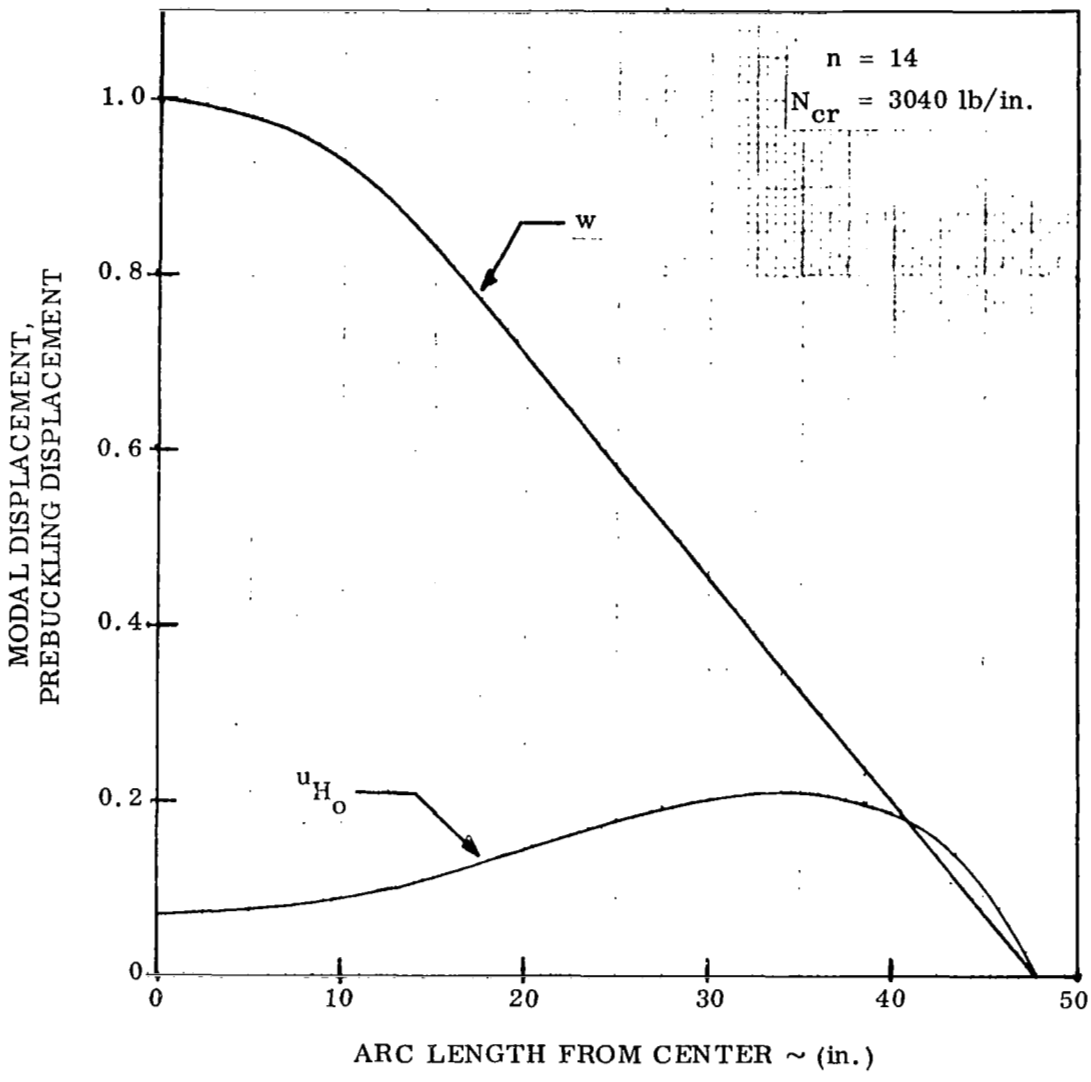

Fig. 4 Prebuckling and buckling displacements of an internally stiffened simply supported cylinder loaded at the centroids of the stiffeners

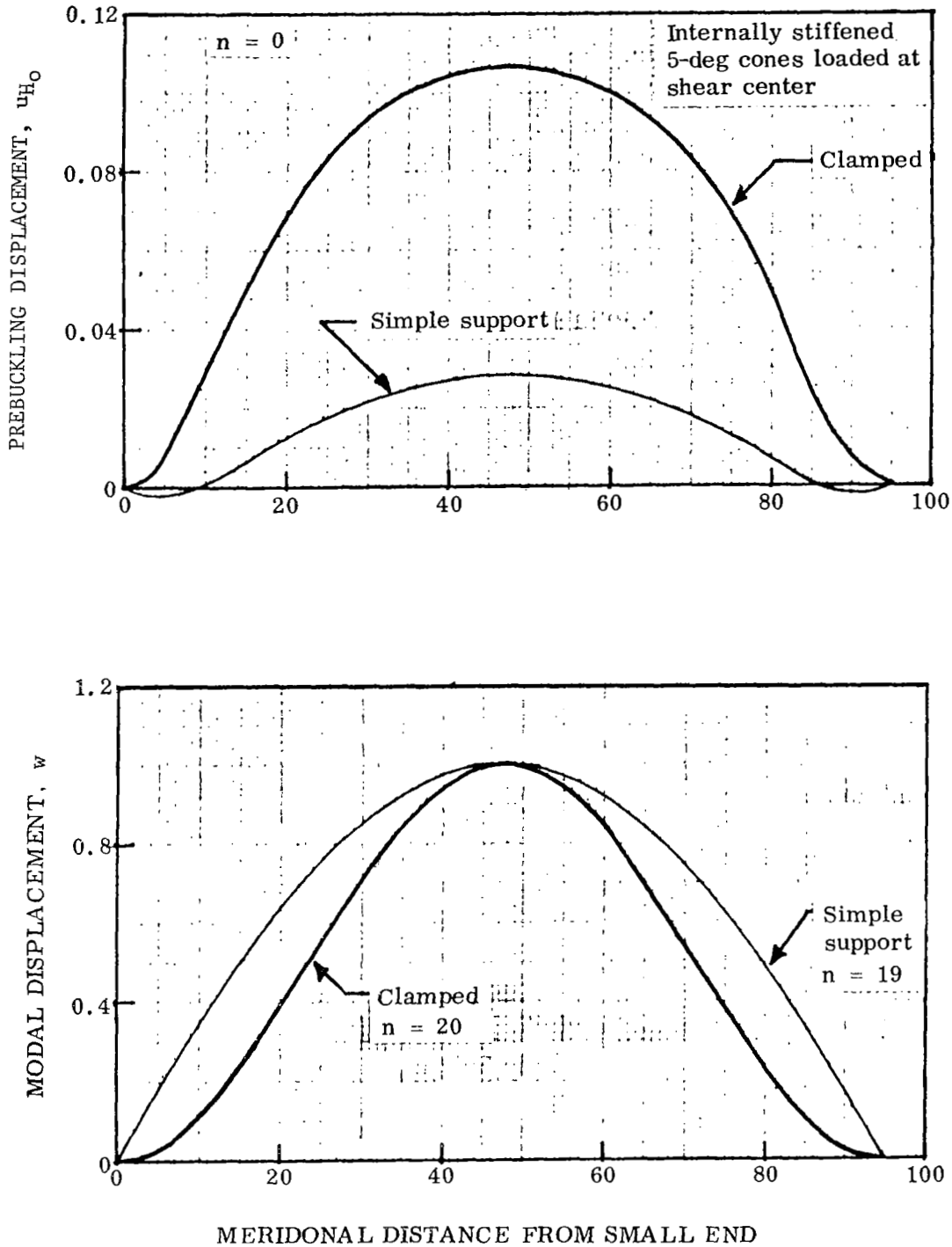

Fig. 5 Prebuckling and buckling displacements of simply-supported and clamped, internally stiffened, 5-deg cones loaded in axial compression through the shear center

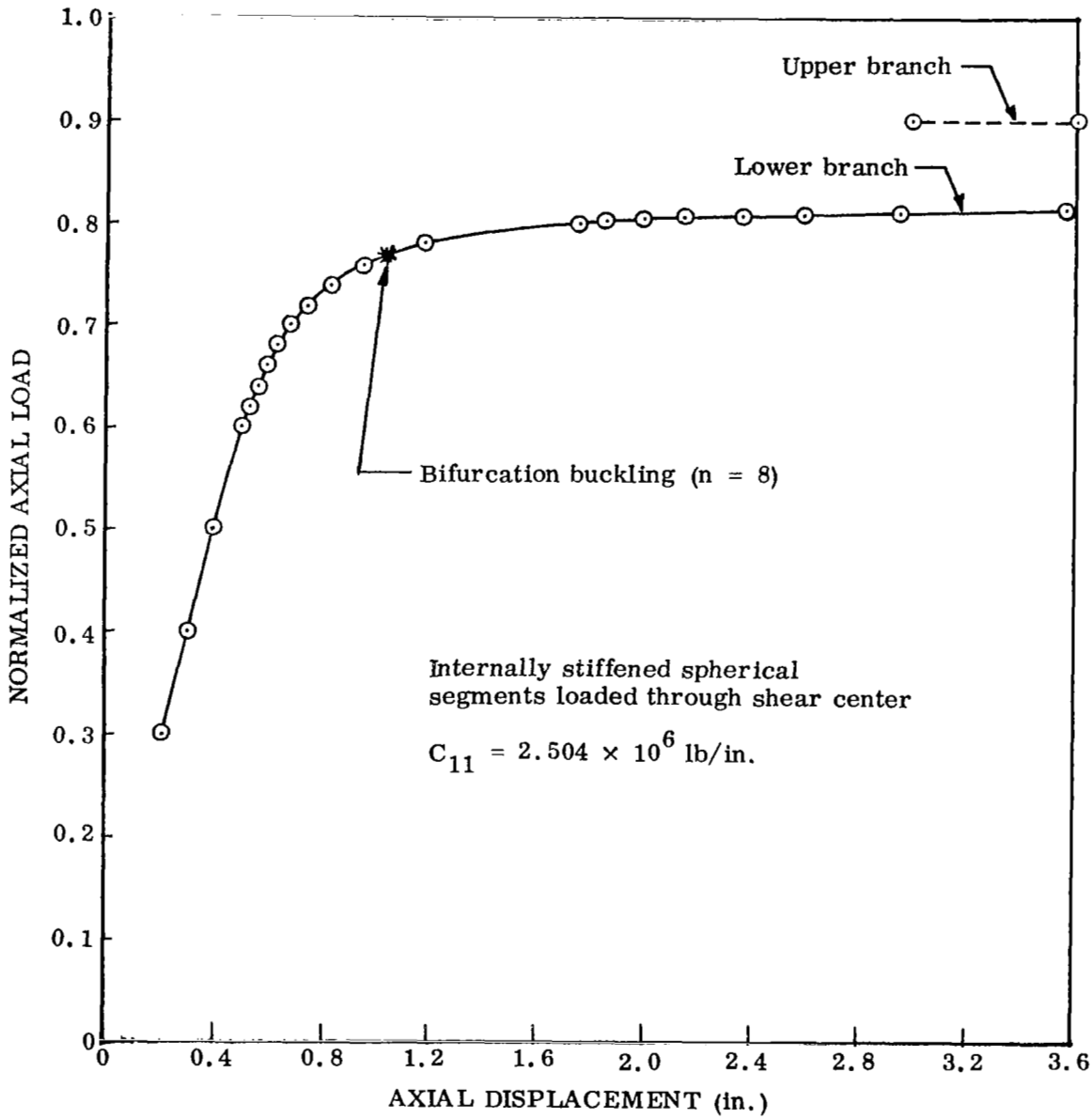

Fig. 6 Prebuckling load-deflection curve for an internally stiffened, simply supported spherical segment loaded in axial compression through the shear center

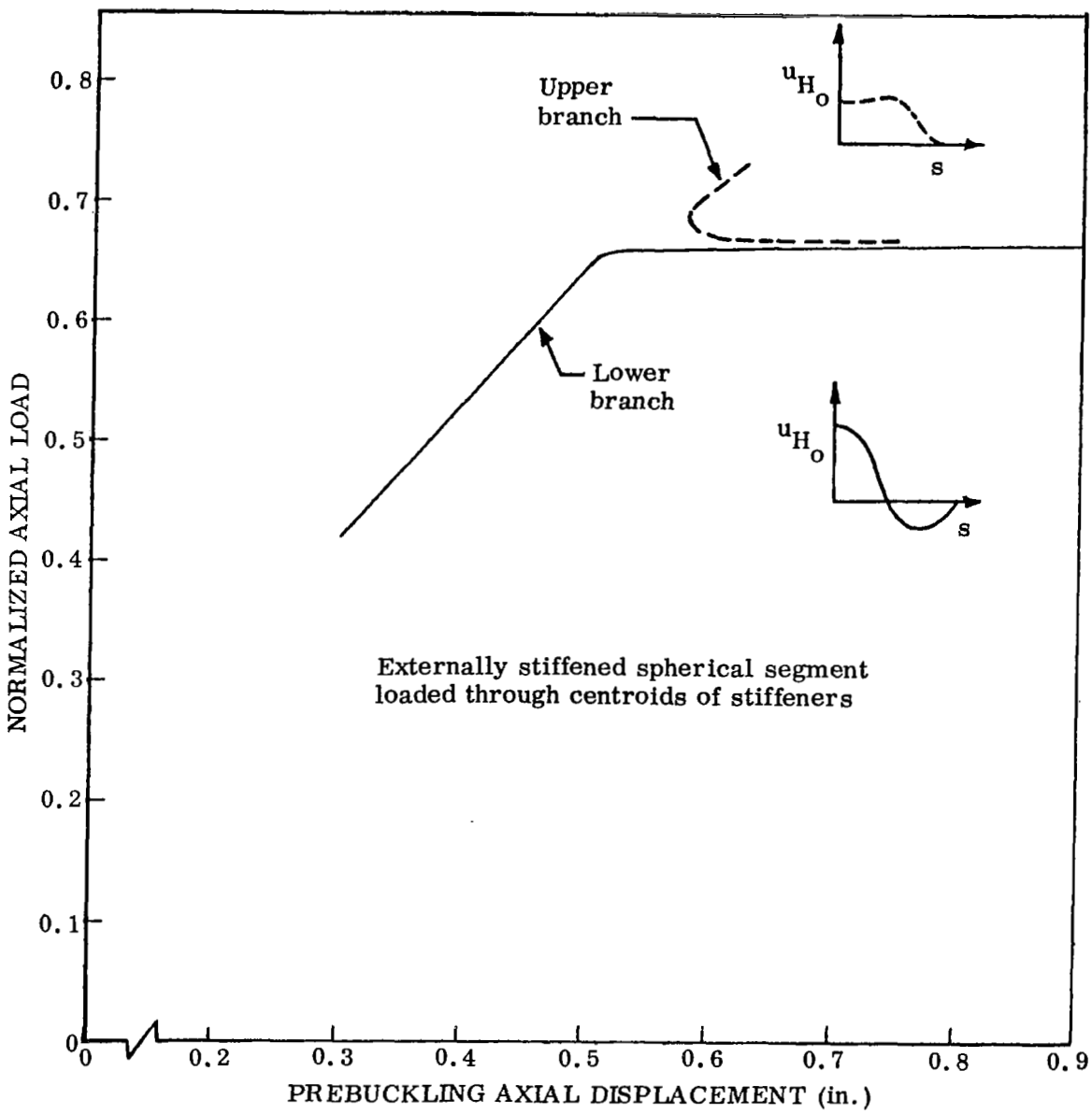

Fig. 7 Prebuckling load-deflection curve for an externally stiffened, simply supported spherical segment loaded in axial compression through the centroids of the stiffeners

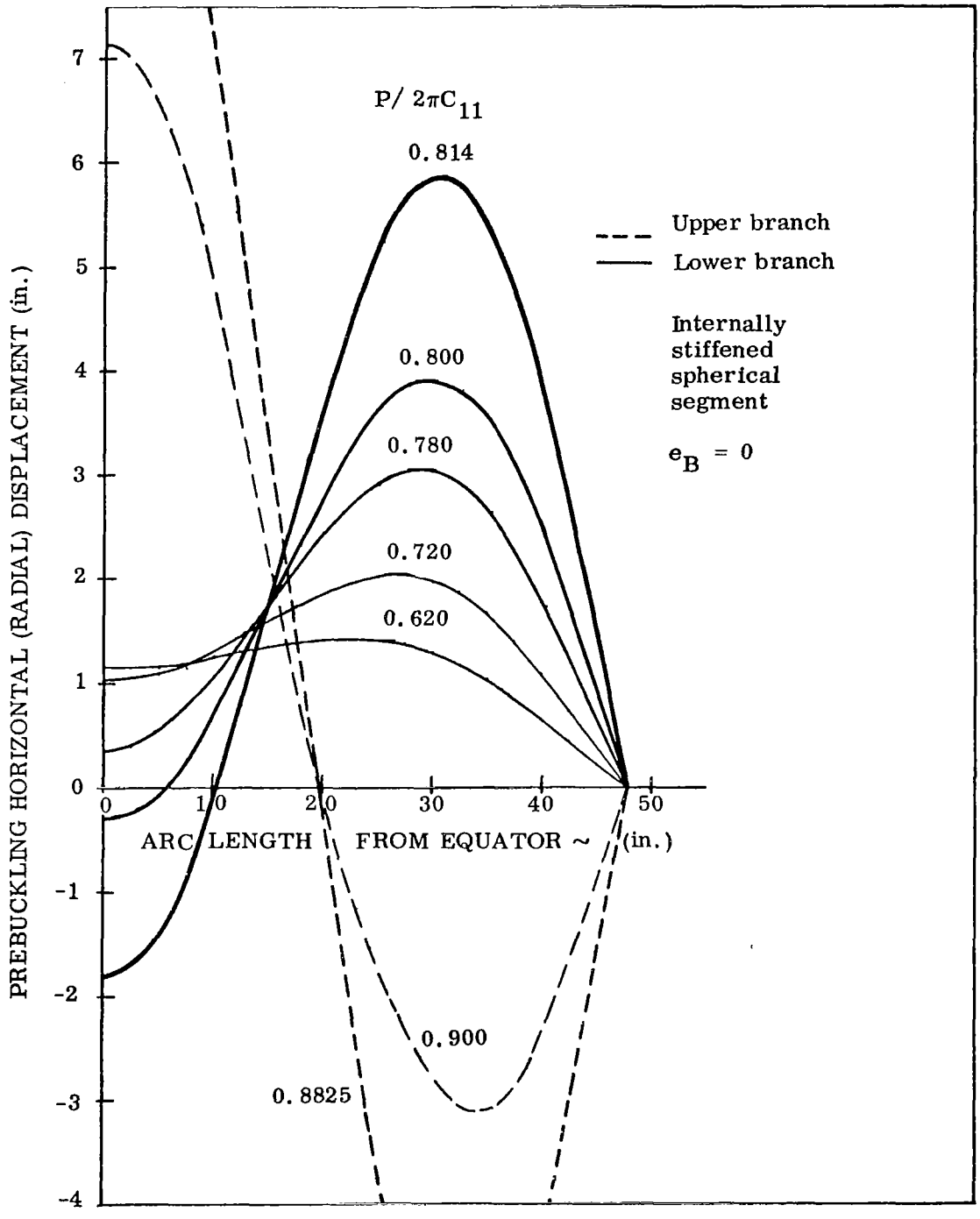

Fig. 8 Prebuckling displacements of an internally stiffened, simply supported spherical segment loaded in axial compression through the shear center

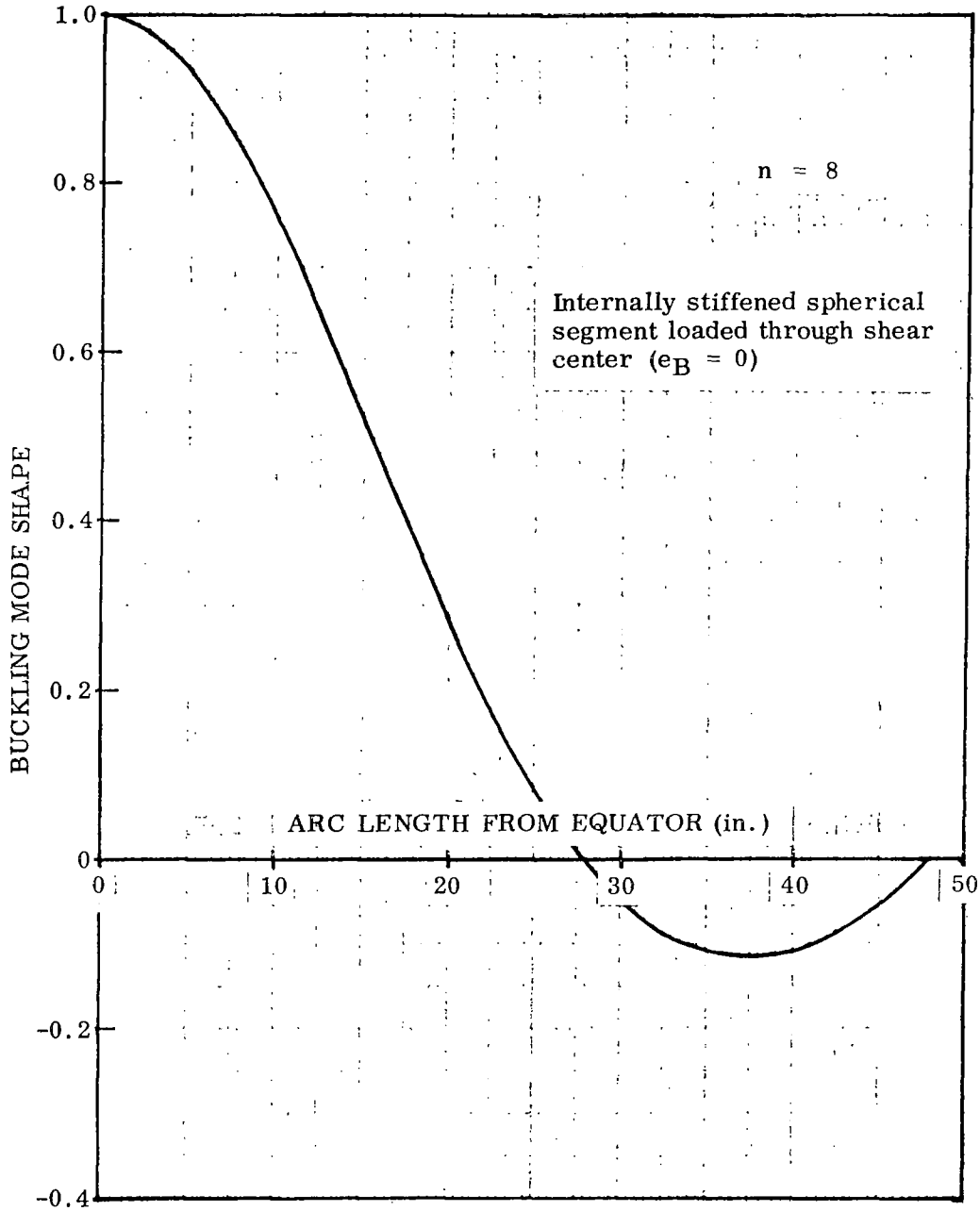

Fig. 9 Buckling mode shape for internally stiffened spherical segment loaded in axial compression through the shear center

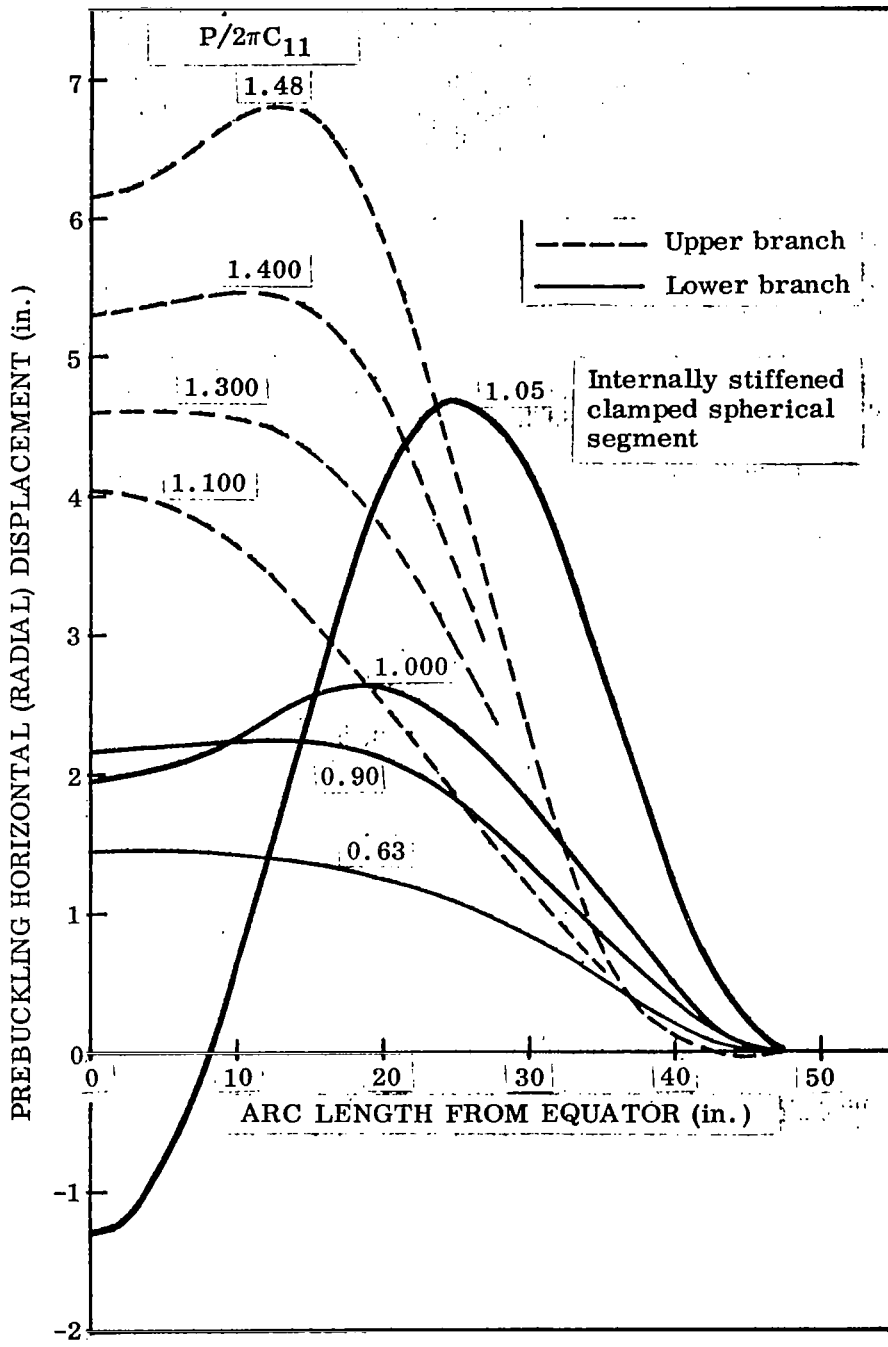

Fig. 10 Prebuckling displacements of an internally stiffened spherical segment loaded in axial compression and clamped at the edges

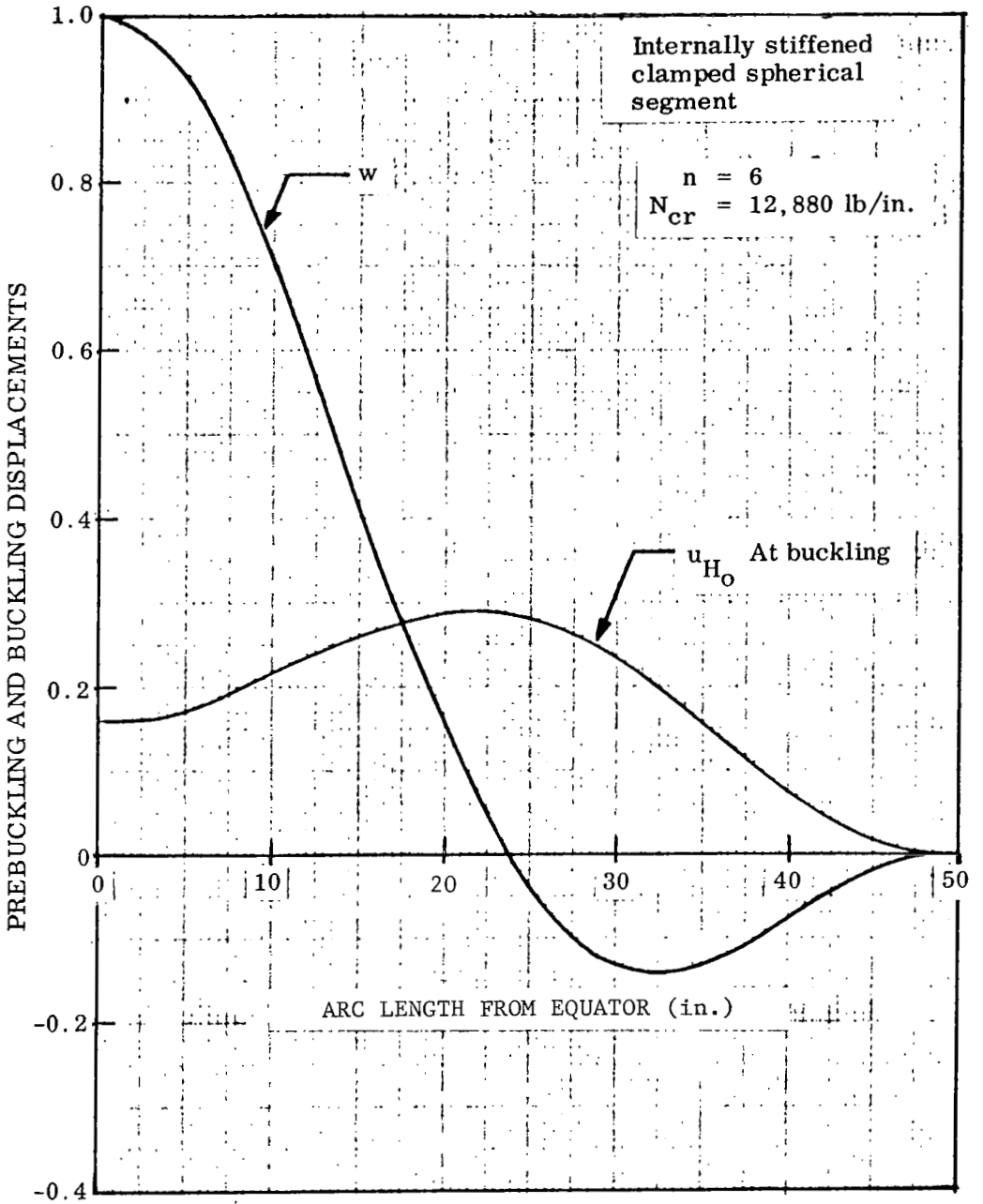

Fig. 11 Prebuckling and buckling displacements of an internally stiffened spherical segment loaded in axial compression and clamped at the edges

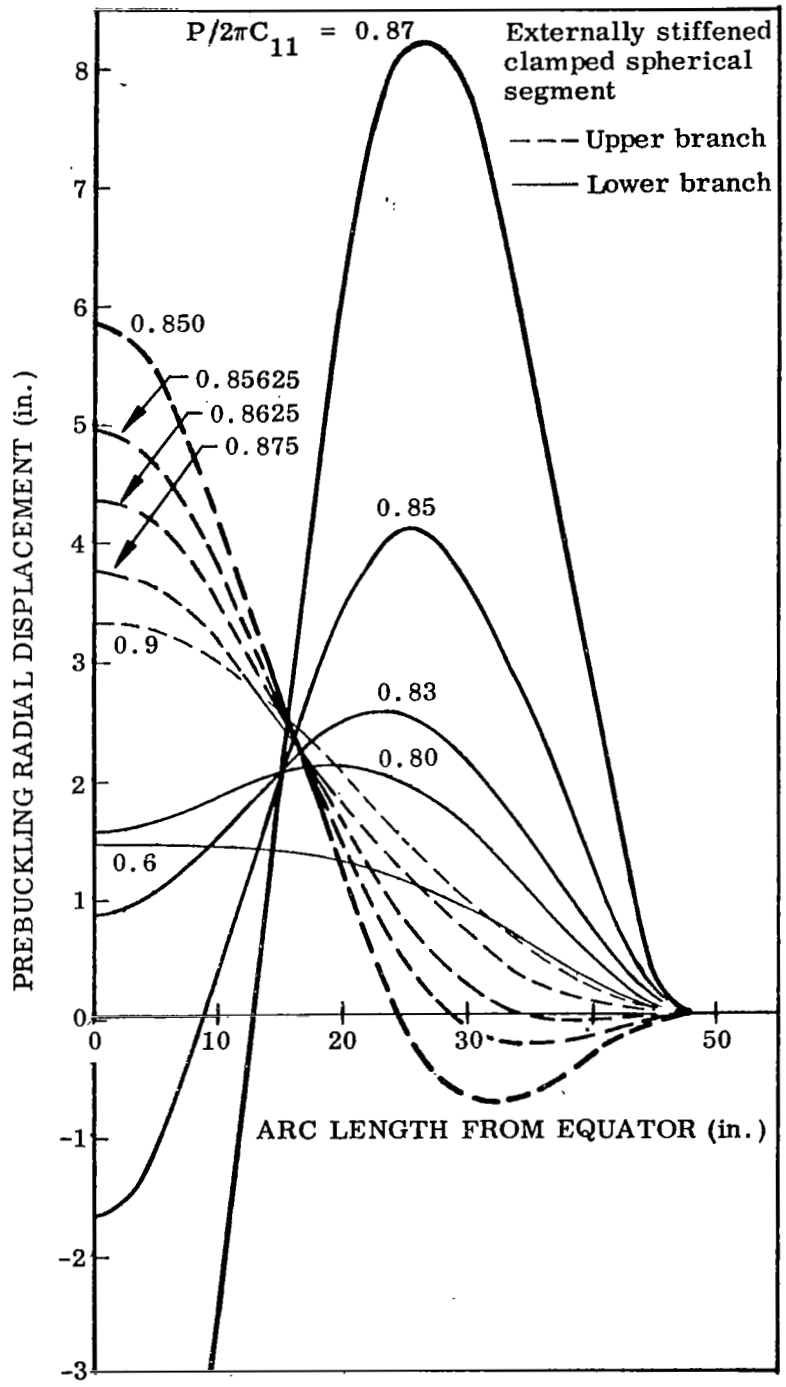

Fig. 12 Prebuckling displacements of an externally stiffened spherical segment loaded in axial compression and clamped at the edges

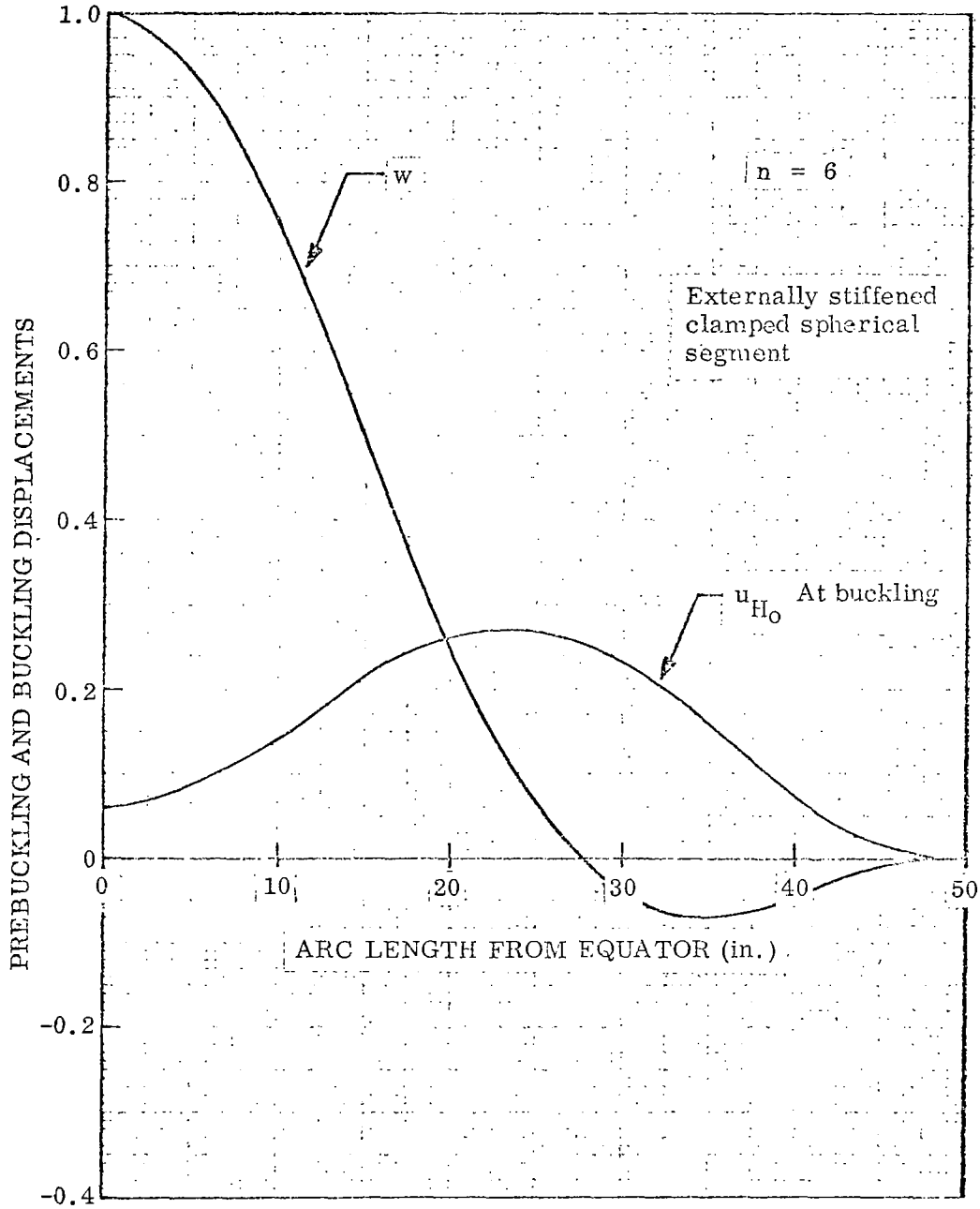

Fig. 13 Prebuckling and buckling displacements of an externally stiffened spherical segment loaded in axial compression and clamped at the edges

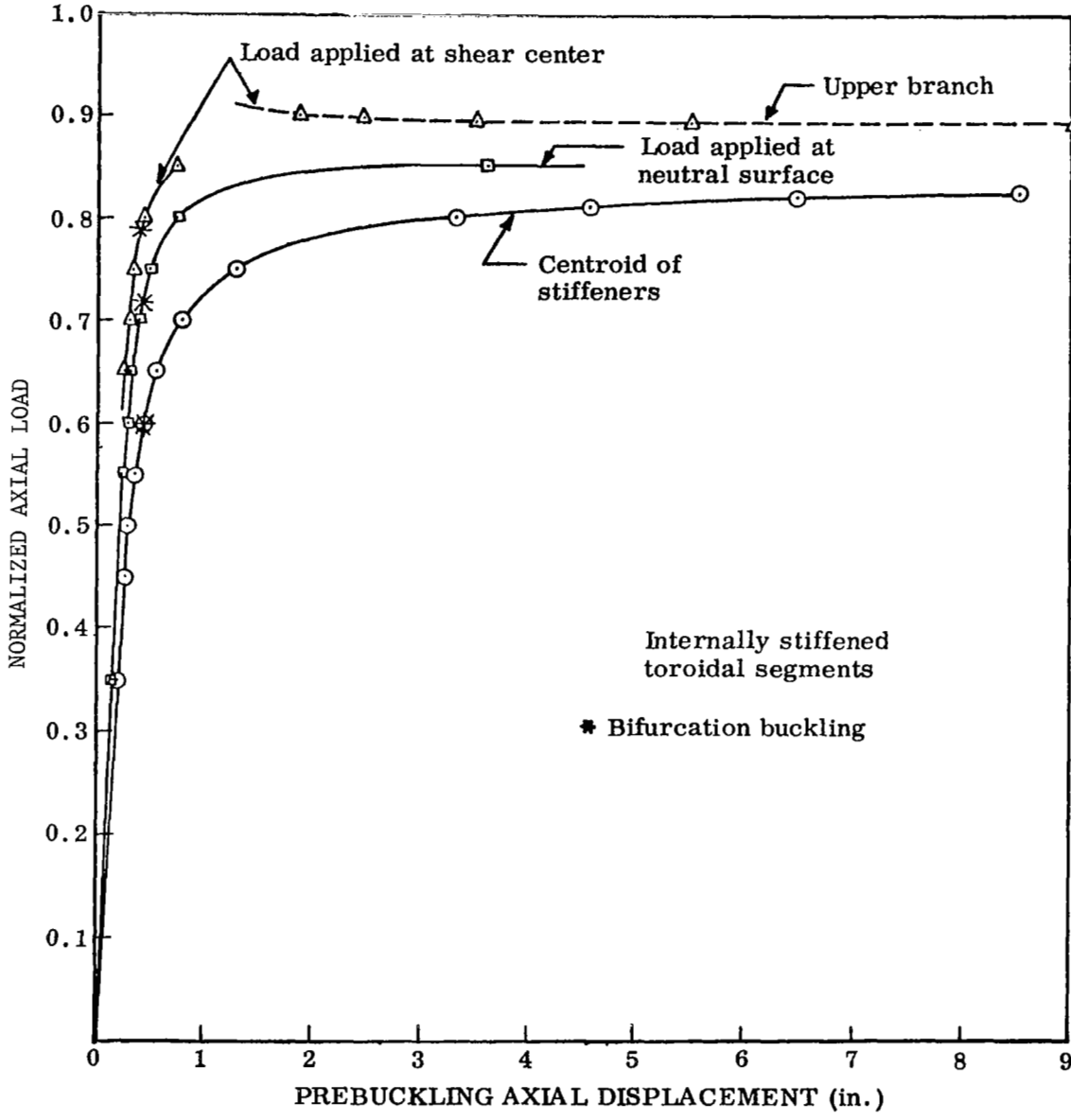

Fig. 14 Load-deflection curves for axially compressed, simply supported toroidal segments

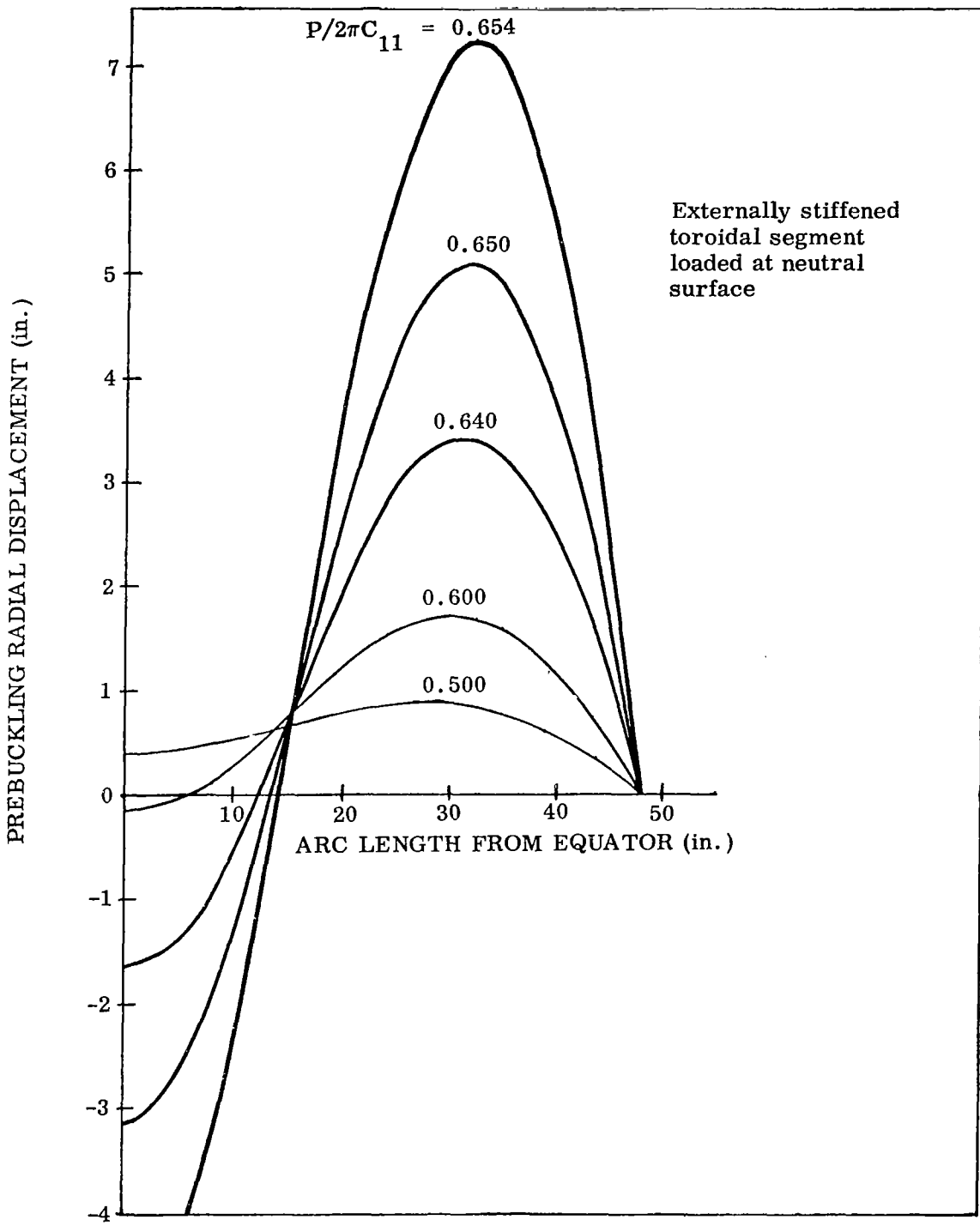

Fig. 15 Prebuckling displacements of externally stiffened, simply supported toroidal segments loaded in axial compression at the neutral surface

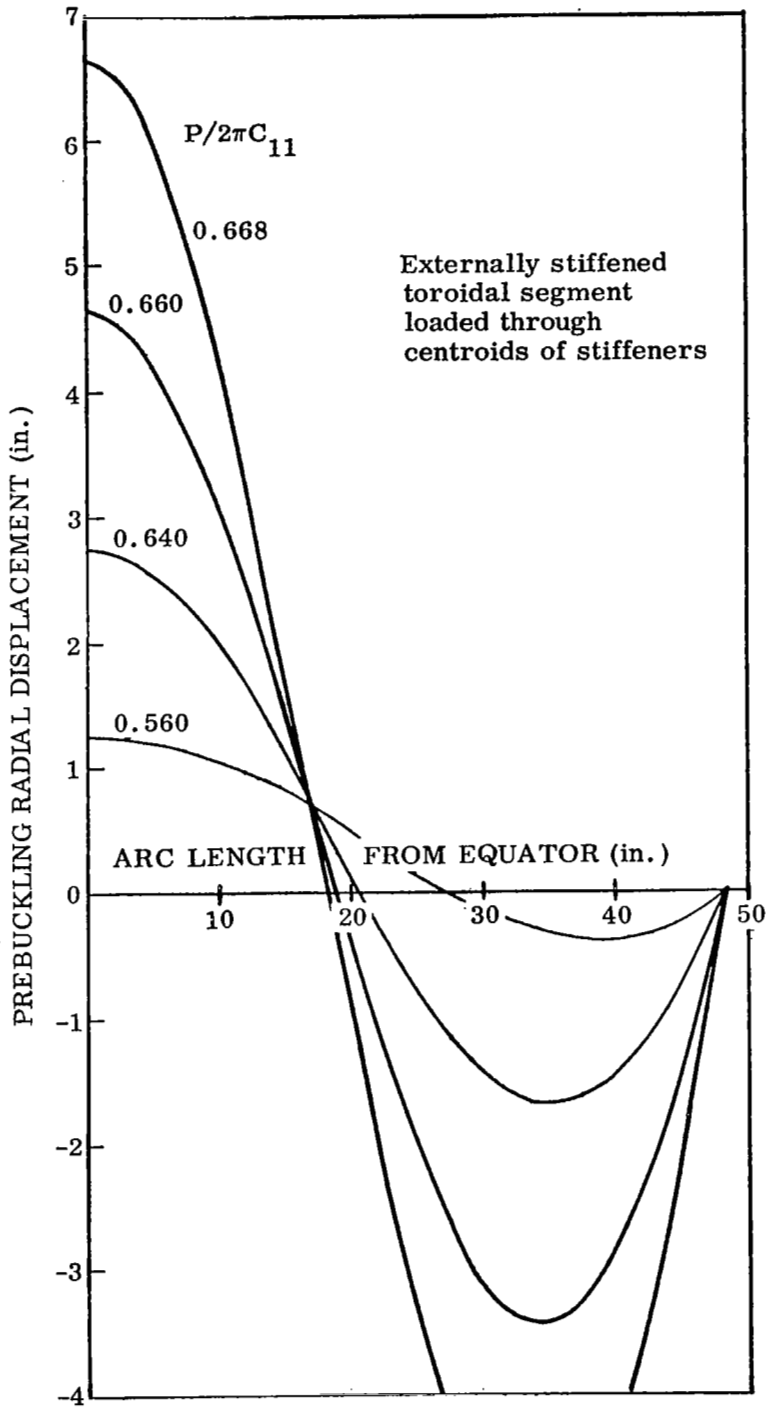

Fig. 16 Prebuckling displacements of externally stiffened, simply supported toroidal segments loaded in axial compression through the centroids of the stiffeners

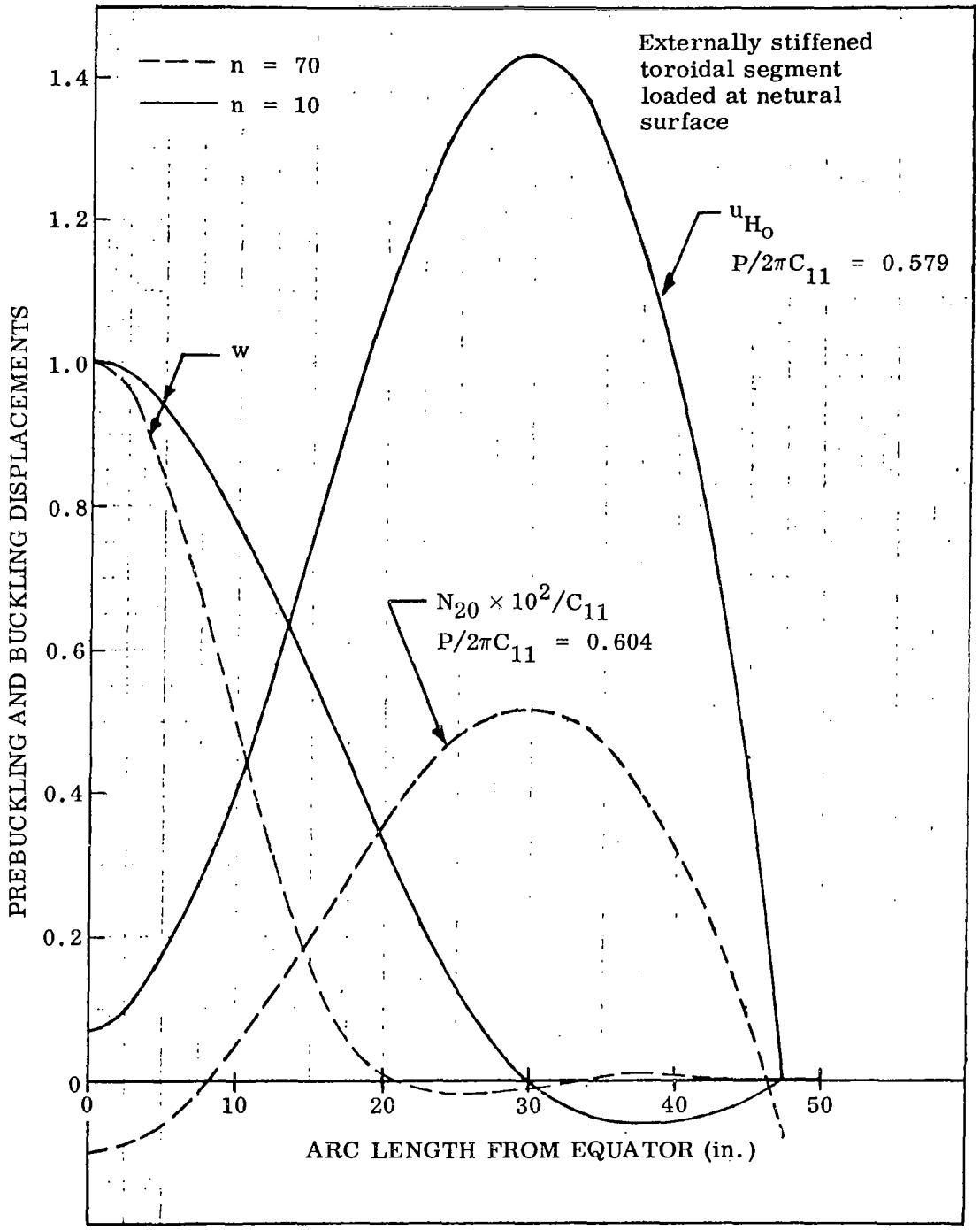

Fig. 17 Prebuckling and buckling displacements and prebuckling circumferential stress resultant for an externally stiffened simply supported toroidal segment loaded in axial compression at the neutral surface

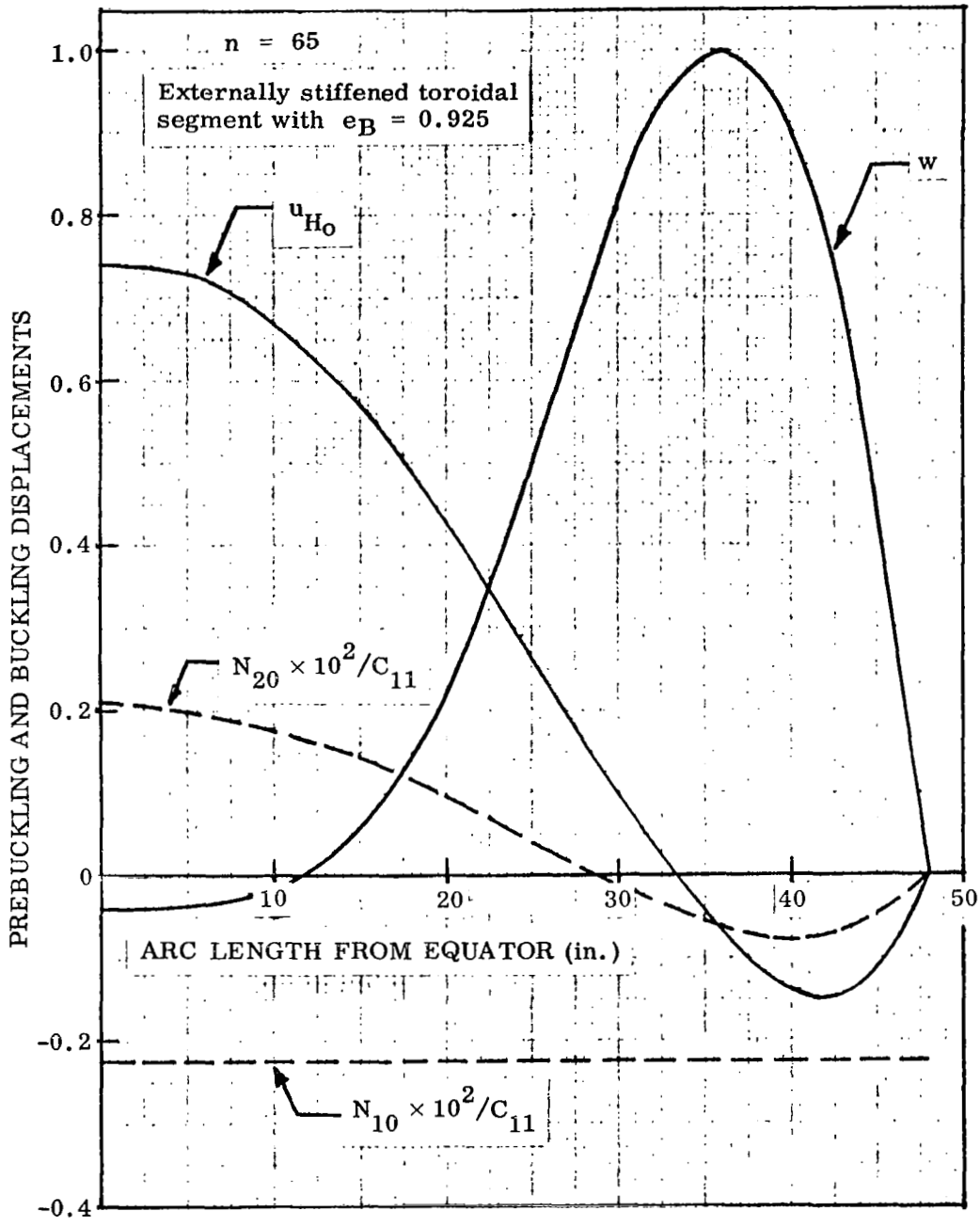

Fig. 18 Prebuckling and buckling displacements and prebuckling stress resultants for an externally stiffened, simply supported toroidal segment loaded in axial compression through the centroids of the stiffeners

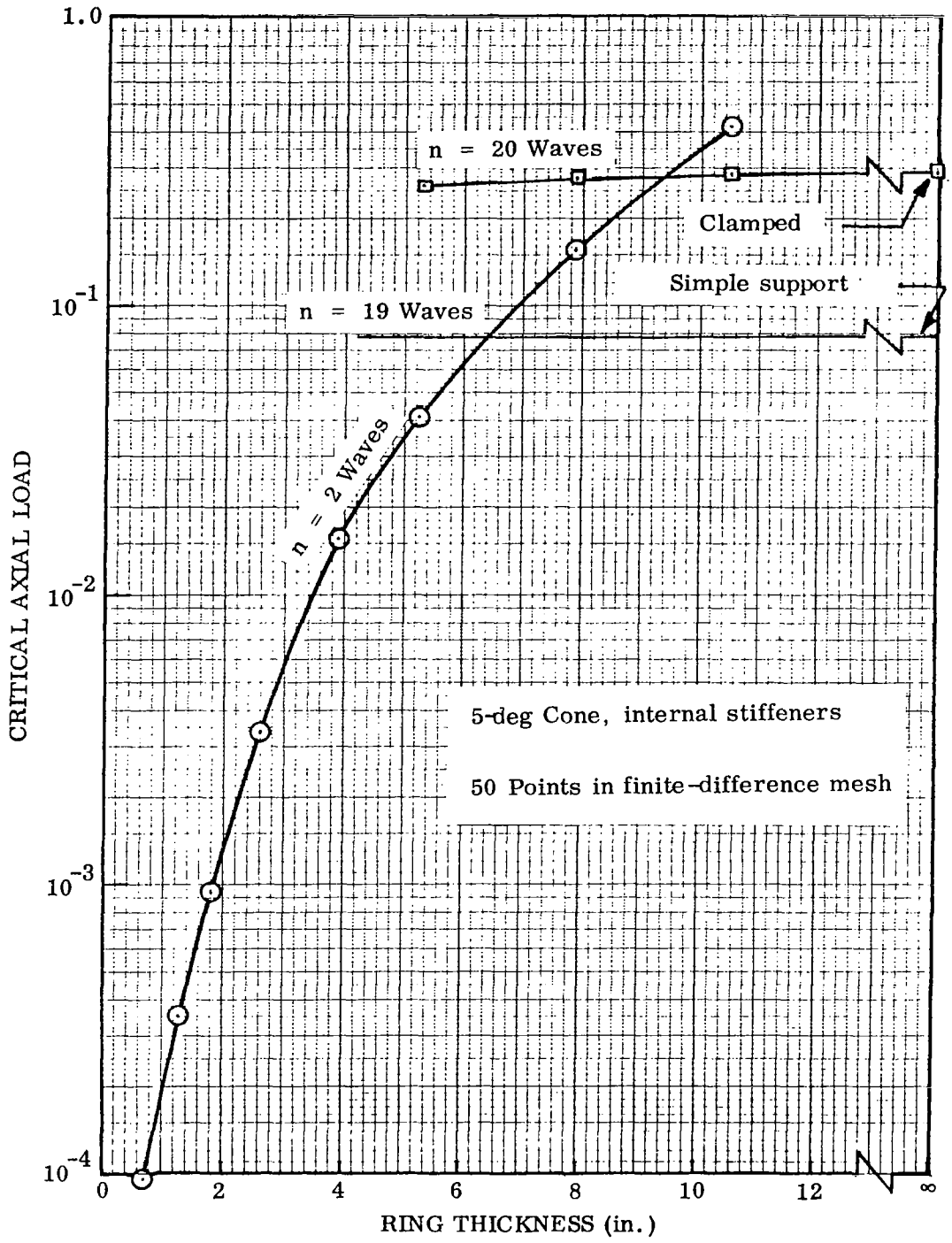

Fig. 19 Critical axial load as a function of ring thickness for cones supported at the edges by rings of square cross section

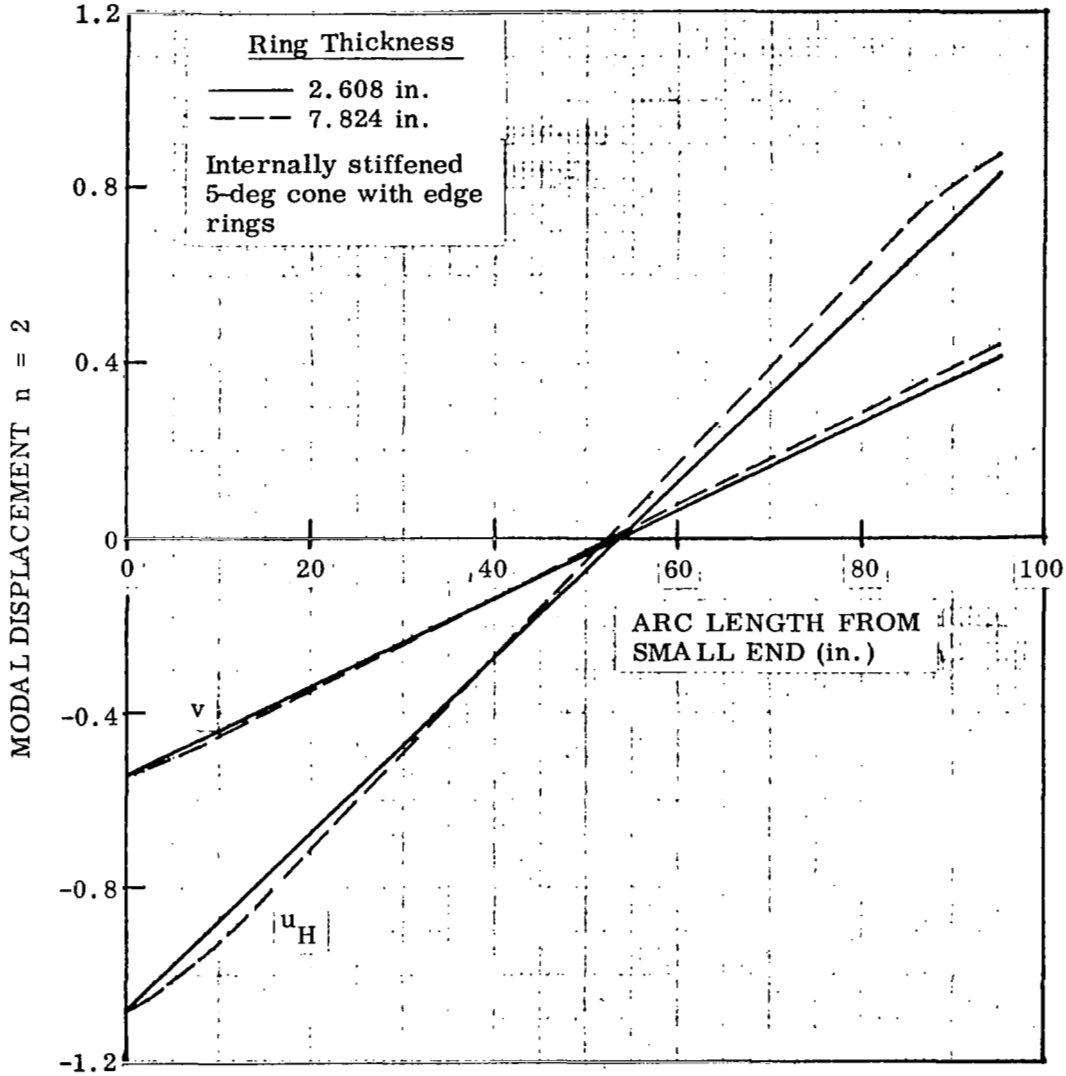

Fig. 20 Modal displacements for ring-supported, internally stiffened 5-deg cones

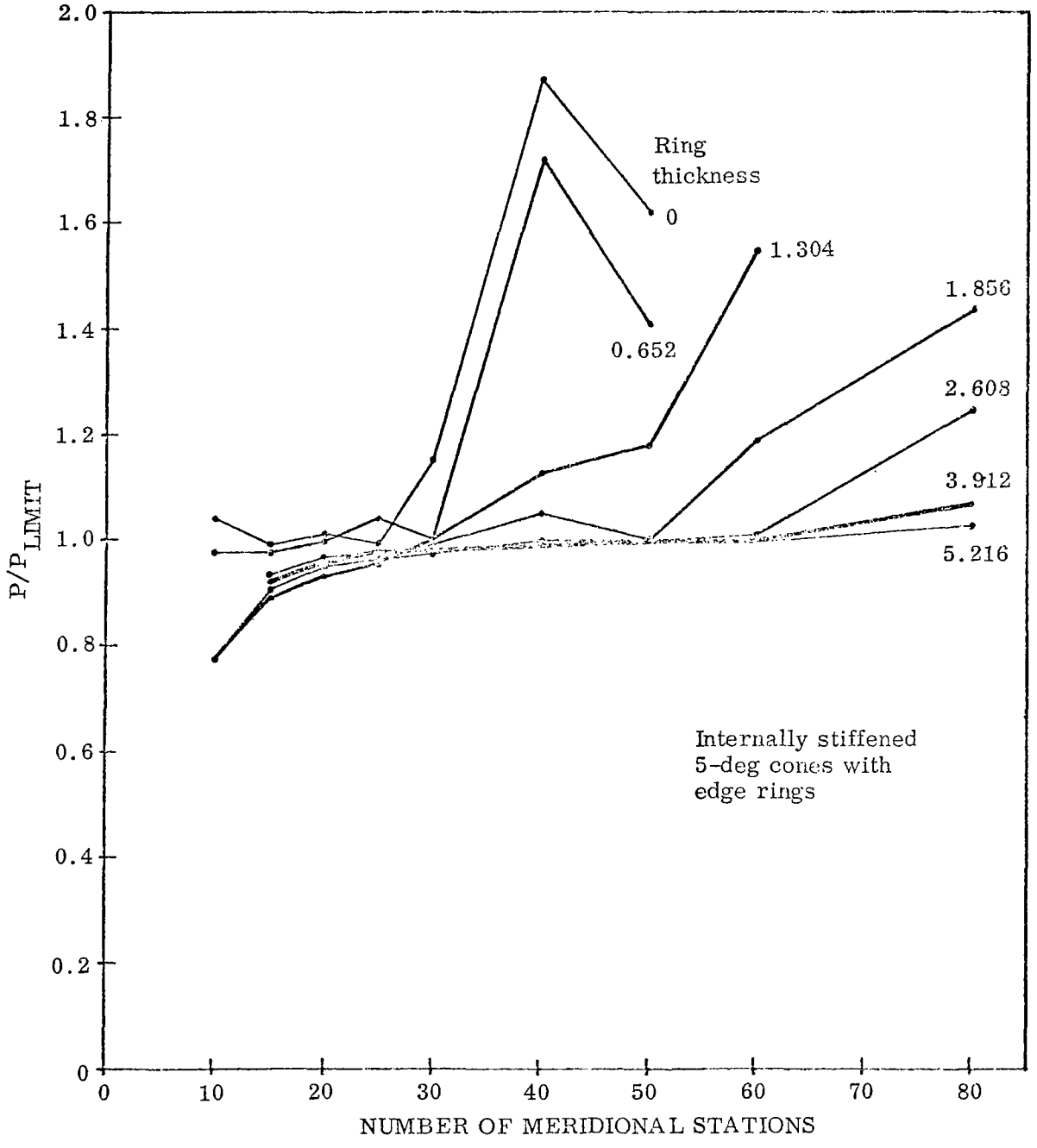

Fig. 21 Critical axial load as a function of number of mesh points for ring-supported internally stiffened 5-deg cones

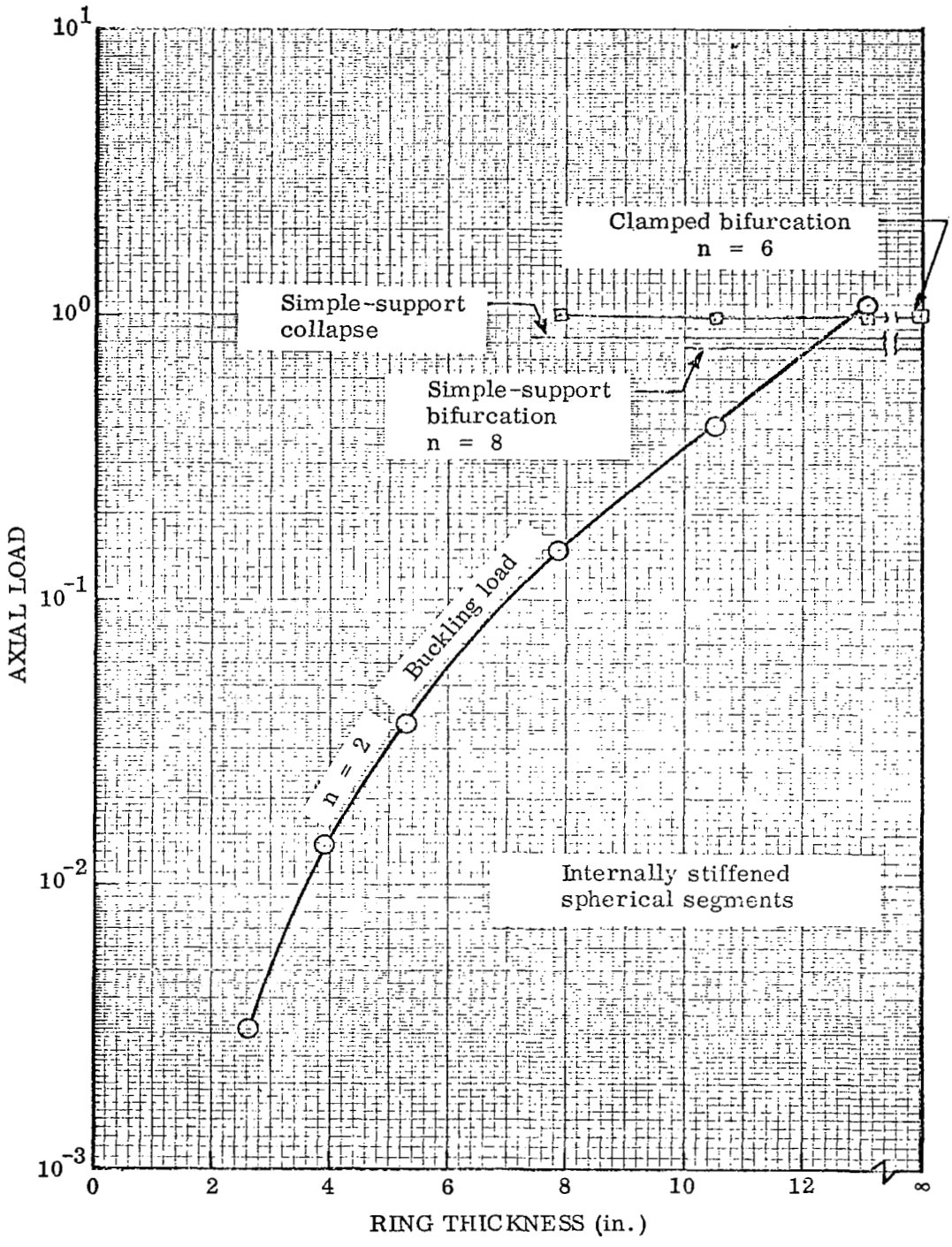

Fig. 22 Critical axial load as a function of ring thickness for internally stiffened spherical segments supported at the edges by rings of square cross section

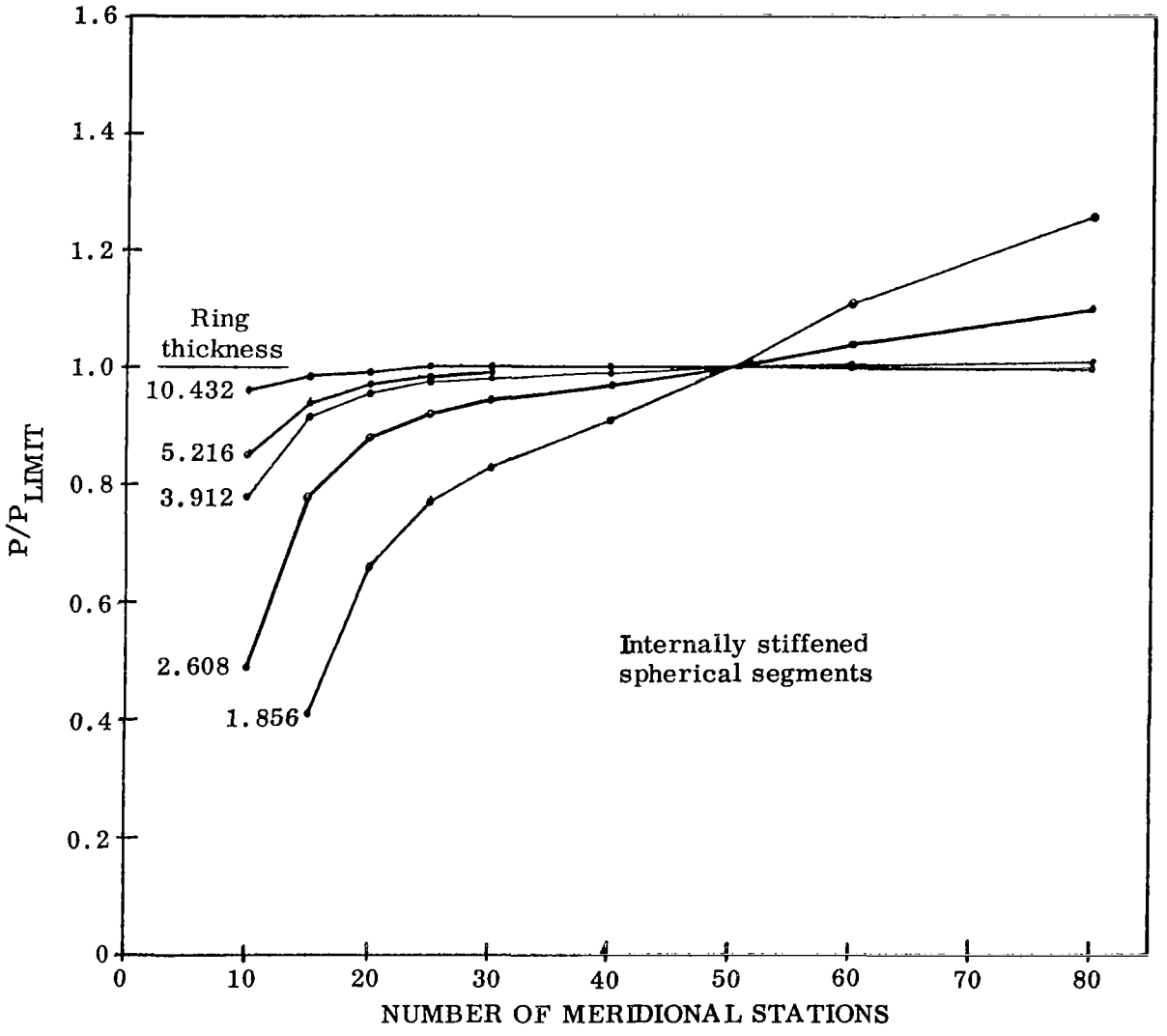

Fig. 23 Critical axial load as a function of number of mesh points for ring-supported spherical segments

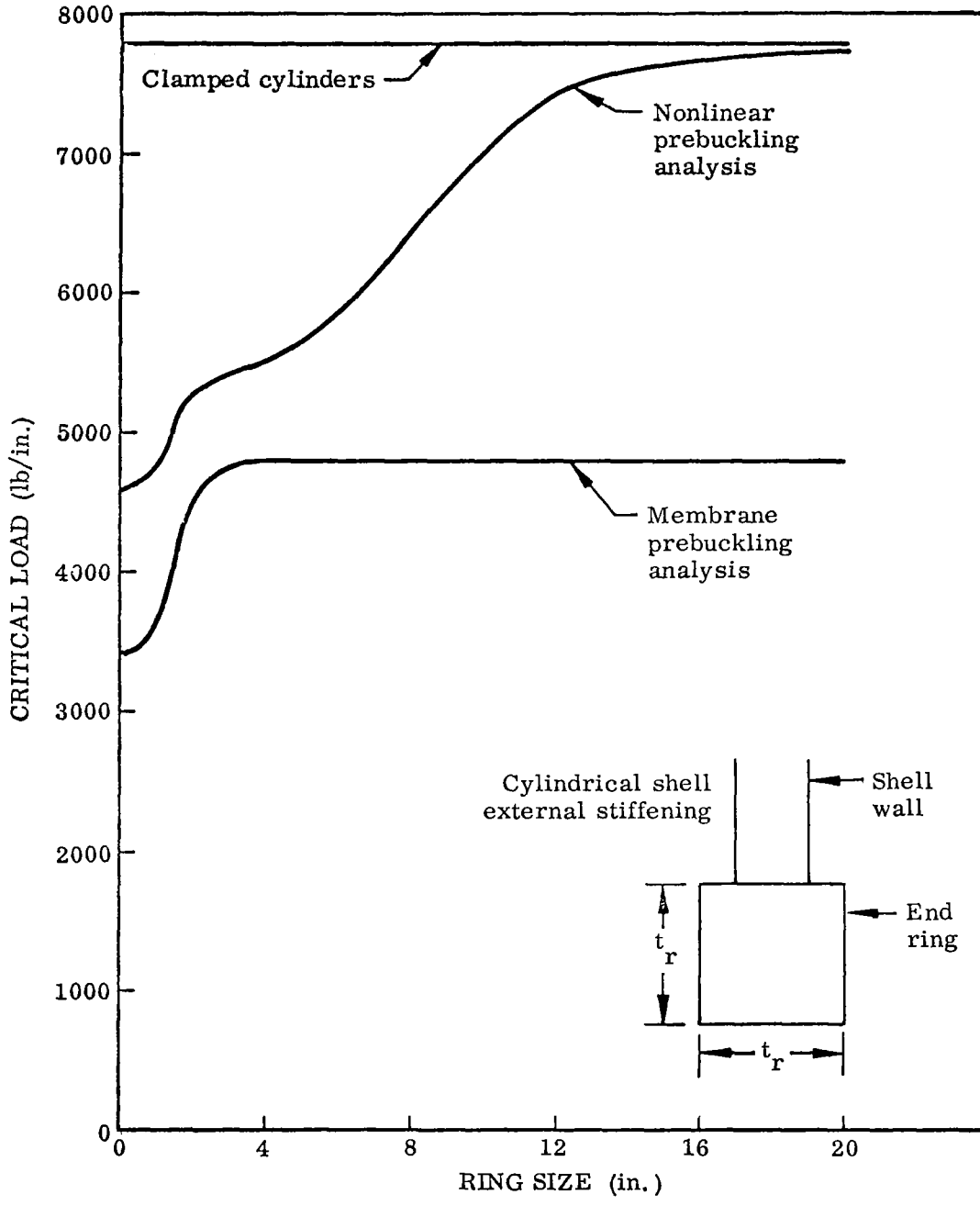

Fig. 24 Influence of ring size on the buckling load for cylindrical shells

NASA-Langley, 1968 — 32 CR-1049